




**sea state**  
cci

## Climate Assessment Report (CAR)

version 3.0, 28 February 2022

		 National Oceanography Centre NATURAL ENVIRONMENT RESEARCH COUNCIL
		
		 SATOC SATELLITE OCEANOGRAPHIC CONSULTANTS
	 CLS COLLECTE LOCALISATION SATELLITES	 IPGP INSTITUT DE PHYSIQUE DU GLOBE DE PARIS
 UNIVERSITAS GALATIENSIS		 IH cantabria INSTITUTO DE HIDRÁULICA AMBIENTAL

Author	Approved	Signature	Date
Guillaume Dodet, Andrew Shaw, Anton Korosov, Christine Gommenginger, Ellis Ash	Fabrice Arduin, Ellis Ash		28 February 2022
<b>ESA Approval</b>			

Issue	Date	Comments
1.0	14/07/2020	First version for ESA review
2.0	18/10/2021	Updates to Case Studies and User Feedback
3.0	28/02/2022	Final updates to Case Studies 1 to 3

## Contents

<b>List of Acronyms</b>	<b>4</b>
<b>1. Introduction</b>	<b>5</b>
<b>2. Case Studies</b>	<b>6</b>
2.1 Case Study 1: Extremes at the coast (NOC)	6
2.1.1 Data & Method	6
2.1.2 Results for High Sea State (Hs >4 m)	7
2.1.3 Results for Low Sea State (Hs <1.5m)	8
2.1.4 Results for all sea states	8
2.1.5 Results for temporal distribution with of inclusion Sentinel 3A / SAR	10
2.1.6 Conclusions and Recommendations	12
2.2. Case Study 2: storm events: extremes & swell	13
2.2.1 Validation of extreme wave heights	13
2.3. Case Study 3: Sea state decadal variability in the North Atlantic	17
2.3.1. Hs climatology	18
2.3.2. Comparison of NA SLP, NA wind intensity, climate modes as sea state predictors	19
2.3.3. Influence of NAO and EA on Hs trends	22
2.4. Case Study 4: Waves in the marginal ice zone (NERSC)	24
2.4.1 Impact of waves on marginal ice zone (MIZ) in 2015	24
2.4.2 Wave climate in the Arctic in relation to marginal ice zone and sea ice extent	28
2.4.3 User Engagement	34
<b>3. Feedback from Sea State Users</b>	<b>35</b>
3.1 Feedback from the First User Consultation Meeting	35
3.1.1 Introduction	35
3.1.2 Group discussion: Climate studies	35
3.1.3 Group discussion: Coastal dynamics	37
3.1.4 Group discussion: Hindcasting and forecasting	37
3.1.5 Group discussion: Marine Engineering	38
3.1.6 Conclusions and recommendations	38
3.2 Feedback from the Climate Research Group	39
3.3 Links with international wave climate activities	39
3.4 Feedback from the Second User Consultation Meeting	40
3.4.1 Introduction	40
3.4.2 Diversity of Audience	41
3.4.3 Interaction	41
3.4.4 Feedback	41
<b>4. References</b>	<b>42</b>

## List of Acronyms

C3S	Copernicus Climate Change Service
CAR	Climate Assessment Report
CCI	Climate Change Initiative
CCO	Channel Coastal Observatory
GCOS	Global Climate Observing System
IOC	Intergovernmental Oceanographic Commission
JCOMM	Joint Technical Commission for Oceanography and Marine Meteorology
MGDR	Merged Geophysical Data Record
MIZ	Marginal Ice Zone
MSW	Maximum Sustainable Wind
RMW	Radii of Maximum Wind
SWH	Significant Wave Height
WCRP	World Climate Research Programme

## 1. Introduction

This document presents the Climate Assessment Report (CAR) for **Sea\_State\_cci**, deliverable 5.1 of the project. This third version was prepared at the end of the project and provides final results of the Case Studies based on CCIv1 and CCIv2 datasets. It also includes feedback from the project Climate Research Group and summarises links with other international wave climate initiatives.

The remainder of this Climate Assessment Report contains a summary of the Case Studies and Feedback from Sea State Users broken down into subsections according to category as follows:

- Section 2: Case Studies:
  - Extremes at the coast
  - Storm events: extremes & swell
  - Links with C3S
  - Waves in the marginal ice zone
- Section 3: Feedback from Users:
  - First User Consultation Meeting
  - Climate Research Group
  - Links with international wave climate activities

## 2. Case Studies

### 2.1 Case Study 1: Extremes at the coast (NOC)

*Andrew Shaw (Skymat Ltd), Ben Timmermans, Christine Gommenginger, Chris Banks (National Oceanography Centre)*

This case study considers wave climate and extremes at the coast, an issue of critical societal relevance - not just for the direct impact of ocean waves on coastal infrastructure and populations, but also for the contribution made by sea state to sea level rise and coastal flooding. The Sea State Climate Change Initiative (CCI) project has released version 2.06 of their satellite altimeter data product. This work investigates the 1Hz along-track measurements provided in v2.06 Level 2P (L2P) products compared with version 1.1. Hereafter, we will refer to CCI Sea State products v1.1 and v2.06 as versions 1 and 2 for brevity.

Timmermans et al. (2020) provided evidence from the Sea State CCI v1 product (10 satellite missions, 1993 to 2018) across six sites of paired wave buoys on the East and West coasts of the USA that showed good overall agreement with buoy data. However, the CCI v1 altimeter record suffers from the low spatial and temporal sampling characteristic of the satellite altimeter constellation, and this was reflected in the underestimation of the 10-year  $H_s$  return levels from the Sea State v1 product. Moreover, Timmermans et al. (2020) reported that the number of valid observations in the CCI v1 altimeter record reduced dramatically within 5 km of the coast.

In this work, these questions are revisited using the CCI V2 altimeter data for two of the six sites of paired wave buoys studied by Timmermans et al. (2020). Expected changes to the CCI v2 altimeter products relate to: a/ retracking of some satellite missions with coastal retrackers (Schlembach et al., 2020) to enhance data recovery and performance near the coast; b/ improved corrections at low sea states and a new calibration has been applied to improve consistency between missions. Finally, a temporal distribution of the total number of good (Quality Flag = 3)  $H_s$  observations per year are displayed including Sentinel 3A / SAR mode from Version 3, based upon a 50 km sampling radius around three new buoy sites (at inshore buoys 41113 and 41010 and offshore buoy 41010).

#### 2.1.1 Data & Method

Analyses focus on two pairs of wave buoys from the National Buoy Data Center (NBDC) in the Maine region (Buoy 44007 inshore, Buoy 44005 offshore) and the Pacific Northwest region (Buoy 46041 inshore, 46005 offshore). The CCI v1 and v2 altimeter datasets were both reduced to limit analyses to the time period common to both releases: 2002-2018.

Standard data quality controls were applied, with  $H_s$  data are considered valid when its corresponding quality flag is equal to 3.

Analyses are based on Level 2 1Hz along-track data for six missions (Envisat, Jason-1, Jason-2, Jason-3, CroSat-2 and Saral AltiKa) that are common to both v1 and v2.

## 2.1.2 Results for High Sea State ( $H_s > 4$ m)

We start by considering the quality of the CCI data in extreme (high) sea states defined by  $H_s > 4$  m. Figure 2.1.1 shows the distribution and data recovery of Significant Wave Height ( $H_s$ ) for high sea states with Sea State CCI products V1 and V2 for the 46041/46005 buoy pairs on the West Coast of the USA. High sea state results are not shown for the East coast site (44007/44005) because the infrequent occurrence of high sea states at that site prevents statistically meaningful analyses.

The results in Figure 2.1.1 show that CCI v2 provides marginally less valid data at high sea states ( $H_s > 4$  m) than V1 at both inshore and offshore sites. The  $H_s$  distributions of the valid satellite data (blue and yellow bars) are reasonably similar to those obtained with buoy observations (red lines). The percentage numbers shown in brackets in the legend indicate the percentage of high sea state observations relative to their corresponding total number of observations for v1 and v2 and the buoys. The percentage numbers of satellite high sea state observations are comparable to the buoy percentages, indicating that the satellite records are correctly capturing the proportion of  $H_s > 4$  m cases at this site.

The 10-year return values for  $H_s$  based on v2 show greater uncertainty than v1 because the time period covered by v2 (2002-2019) is considerably shorter than v1 (1993-2018). Since the low sampling in v1 resulted in underestimated  $H_s$  10-year return levels (Timmermans et al., 2020), the return values for v2 are not provided.

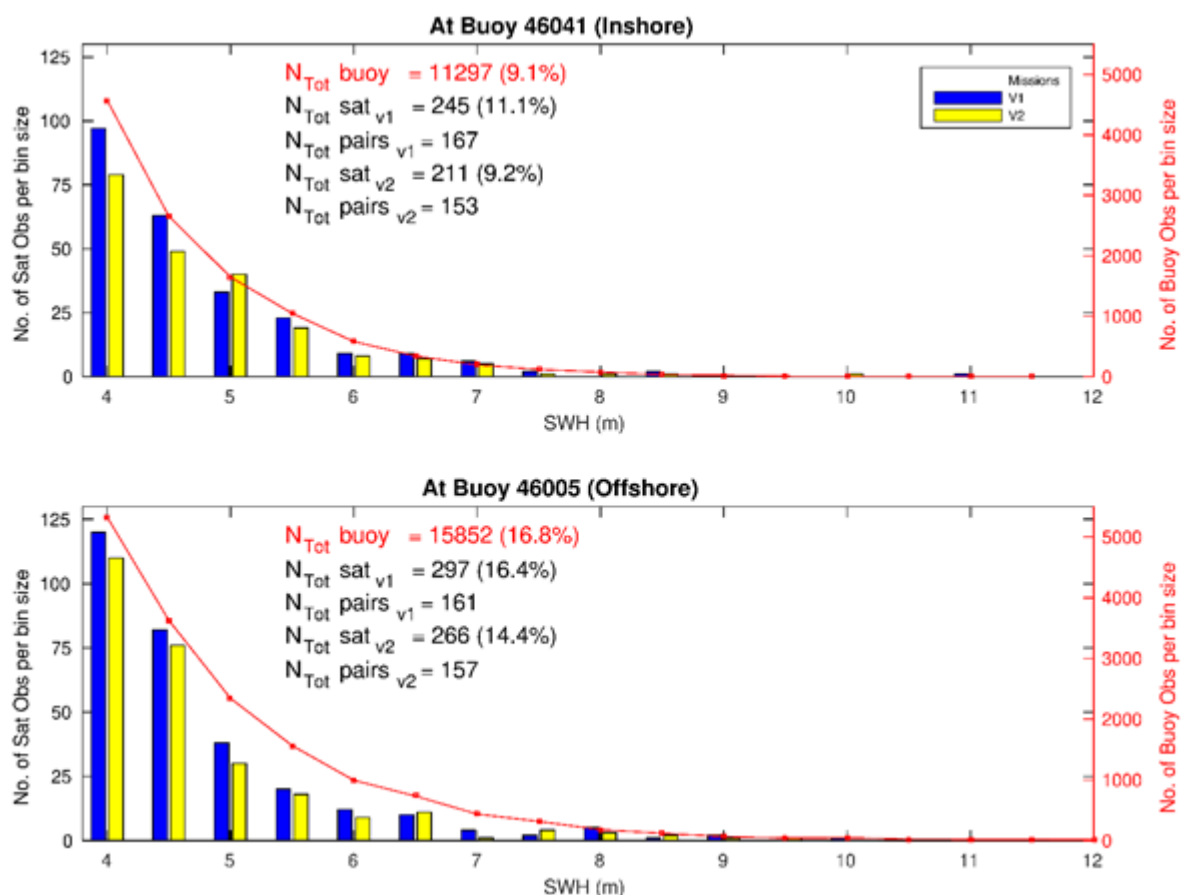


**Figure 2.1.1** Distribution and data recovery of Significant Wave Height ( $H_s$ ) for high sea states ( $H_s > 4$  m) with Sea State CCI products V1 and V2 for the 46041/46005 buoy pairs on

the West Coast of the USA. Satellite data correspond to five altimeter missions (Envisat, Jason-1, -2, -3, CryoSat-2 and Saral) for the period of 2002 to 2018. Bin size is 0.5m.  $N_{tot}$  buoy is the total number of buoy Hs observations above 4m.  $N_{tot} sat_{v1}$  and  $N_{tot} sat_{v2}$  are the total number of Hs observations above 4 m for the CCI v1 and v2 products.  $N_{tot} pairs_{v1}$  and  $N_{tot} pairs_{v2}$  are the total number of valid satellite observations collocated with valid buoy observations (50 km, hourly bins). The percentages in brackets represent the proportion of Hs data above 4 m relative to the total number of observations.

### 2.1.3 Results for Low Sea State (Hs <1.5m)

The number of Hs observations obtained at low sea state (Hs < 1.5m) for the buoys, CCI v1 and CCI v2 datasets are shown in Table 2.1.1 for the period 2002 to 2018.

The results indicate that CCI v2 data contain more low sea state observations than v1 on the west coast of USA, but a decrease on the east coast of USA. The percentage of v2 valid low sea state samples (relative to the total number of samples) on the west coast of USA increases noticeably, particularly at the inshore buoy location (inshore 46041 +17% and offshore 46005, +13%). However, these findings are reversed on the east coast of USA where v2 decreases, 45005, -5%, offshore (44005, -2%) compared with v1.

**Table 2.1.1** Number of Low Sea State Hs observations (Hs <1.5 m) for the period 2002 to 2018 for Sea State CCI product v1 and 2 and their corresponding buoy sites.

	East Coast USA		West Coast USA	
	44007 Inshore	44005 Offshore	46041 Inshore	46005 Offshore
$N_{Tot}$ buoy	116,837	71,081	38,977	17,750
$N_{Tot}$ sat v1	929	1,307	607	262
$N_{Tot}$ sat v2	883	1,278	710	297

### 2.1.4 Results for all sea states

We now consider the CCI v1 and v2 Hs for satellite data collocated with buoys (50 km, hourly bins). Figure 2.1.2 shows the distributions (red histograms) and median values of 'buoy minus satellite' Hs differences (black lines) as a function of buoy Hs for the two CCI products. We find that the probability distributions and the number of valid observations (shown in the subplot titles) are very similar for CCI v1 and v2 for all sites.



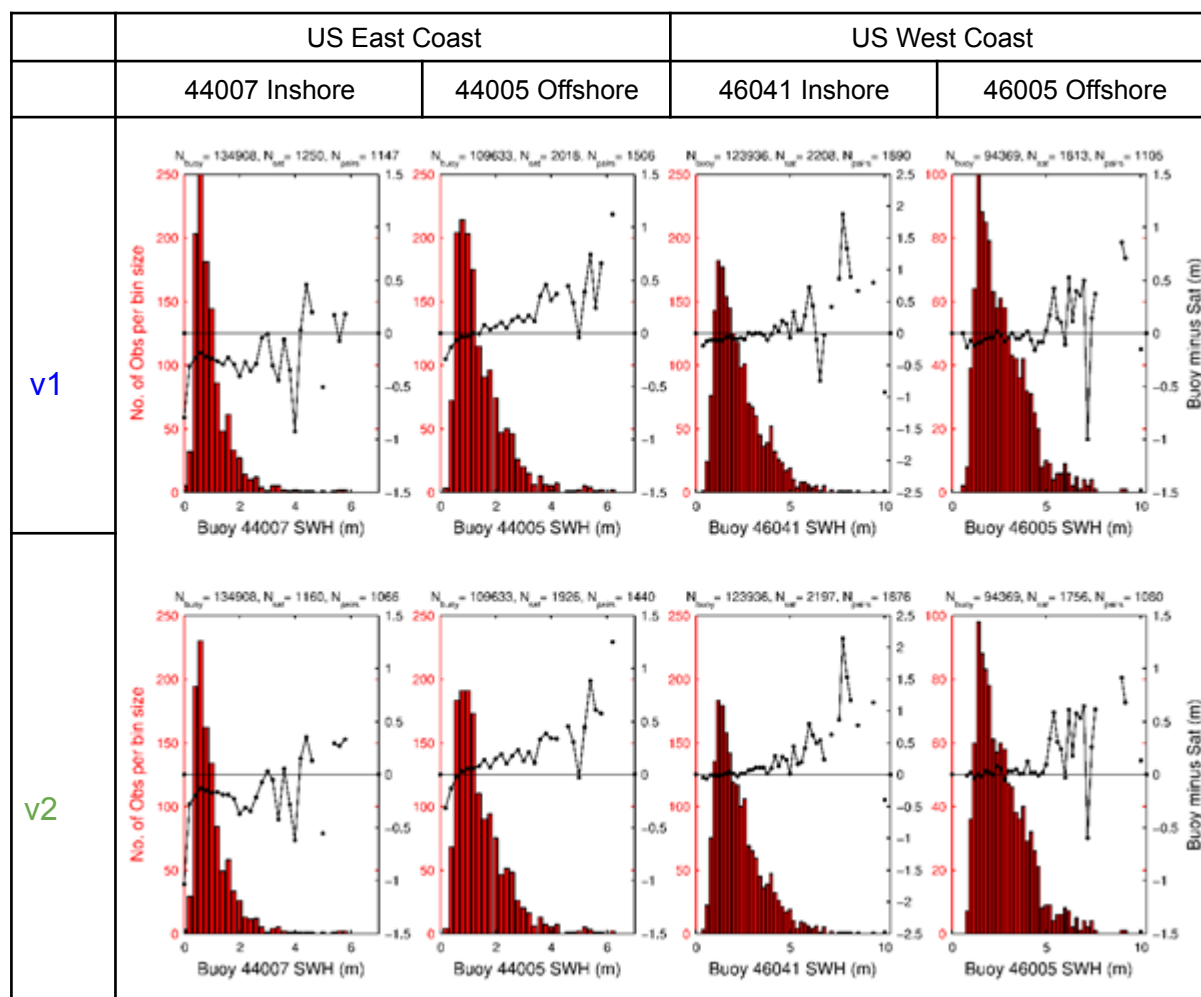


**Figure 2.1.2 2** Distributions (red) and median values of ‘buoy minus satellite’ differences across all sea states for CCI v1 (top panels) and v2 (bottom panels). Satellite data correspond to five altimeter missions (Envisat, Jason-1, -2, -3, Cryosat-2 and Saral) for the period of 2002 to 2018. Figures in the subplot titles are:  $N_{buoy}$  is the total number of valid buoy observations,  $N_{sat}$  gives the total number of valid satellite observations and  $N_{pairs}$  displays the total number of collocated buoy and satellite observations per buoy location for V1 and V2. The bin size is 0.2m. Note the different  $H_s$  limits (x-axis) for buoys on the US East and West coasts.

Minor differences are seen in the bias between the satellite data and the buoys (black lines) for CCI v1 and v2. Across all sea states, the biases show a general positive shift (upwards) for v2 compared with v1. This results in slightly smaller biases between v2 and buoys at low sea states, but marginally larger biases at high sea states.

This is confirmed by the figures in Table 2.1.2 showing the median difference for low and high sea states (values in square brackets). The median difference is systematically lower for v2 than v1 in low sea states, and systematically higher for v2 than v1 in high sea states. However, the high sea states median values are based on relatively small numbers of samples, therefore a larger dataset would be needed to confirm this result.

The RMS differences show consistent values for v1 and v2 (Table 2.1.2), including the noticeably larger RMS difference at buoy 46041 (US West coast, inshore) in both products.

**Table 2.1.2** Root-mean-square and median of ‘buoy minus satellite’ differences for CCI v1 and v2 Hs collocated with buoys. The values in square brackets represent the median difference for low sea state (buoy Hs <1.5m) and high sea state (Hs > 4 m).

Location	RMS difference (m)		Median difference (m)	
	v1	v2	v1	v2
East inshore 44007	0.35	0.34	-0.25 [-0.25, 0.10]	-0.18 [-0.18, 0.21]
East offshore 44005	0.35	0.39	0.11 [-0.04, 0.38]	0.18 [0.03, 0.45]
West inshore 46041	0.51	0.58	-0.01 [-0.11, 0.20]	0.11 [-0.02, 0.44]
West offshore 46005	0.30	0.33	-0.02 [-0.09, 0.13]	0.04 [-0.01, 0.25]

### 2.1.5 Results for temporal distribution with of inclusion Sentinel 3A / SAR

The multi-mission temporal distribution of good Hs observations (Quality Flag = 3) is shown in Figures 2.1.3a to 2.1.3c. Each timeseries is positioned around a pre-existing buoy site having a sampling radius of 50 km. Three buoy sites are chosen, two inshore and one offshore. The data are binned yearly for the period January 2002 to December 2020. The temporal plots show that inshore buoys have a lot less data (Fig. 2.1.3a & c) compared with Fig. 2.1.3b offshore. This data loss inshore is due to the proximity of land cover and the increase in the rejection flags close to the coast (Timmermans *et al.* 2020). It has been noted that there are very little or no data beyond 2008 from Jason-1 at buoy site 42035 (Fig. 2.1.3c). However, this may be explained as Jason-1 orbit was moved to an interleaved trajectory with Jason-2 at the end of repeat cycle 259 (26 January 2009). Very little Cryostat-2 data are shown in Figure 2.1.3a (Buoy41113) because the satellite is operating in SAR mode.

The later years from the combined dataset from v2 and v3 provide more data than the earlier period, although some data from Jason-3 and Saral AltiKa were not available after mid-2019 and 2020. The increasing amount of recent data is good for oceanographic studies; however, it is the long-term timeseries data that includes the earlier missions (ERS-1, TOPEX, ERS-2, GFO and Envisat) that are needed for climate studies.

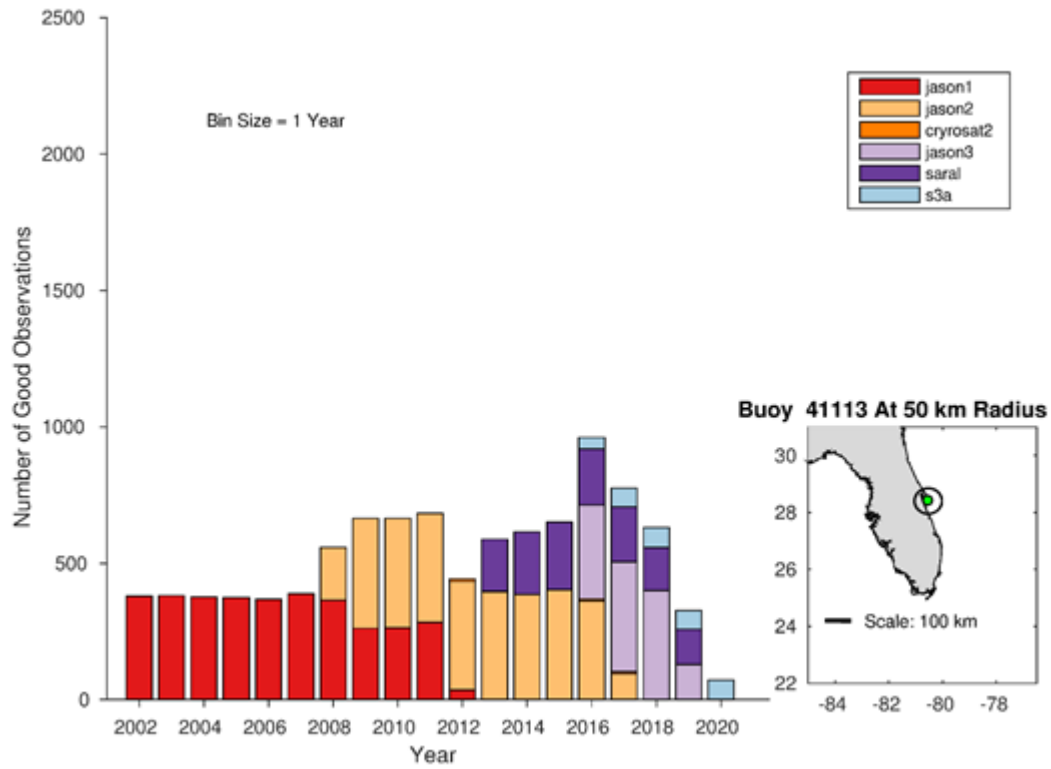


**Figure 2.1.3a** Temporal distribution (Jan 2002 to Dec 2020) of good observations (Quality Flag =3) of v2.06 and Sentinel 3A / SAR (v3) of the Sea State CCI multi- mission dataset at Buoy 41113.

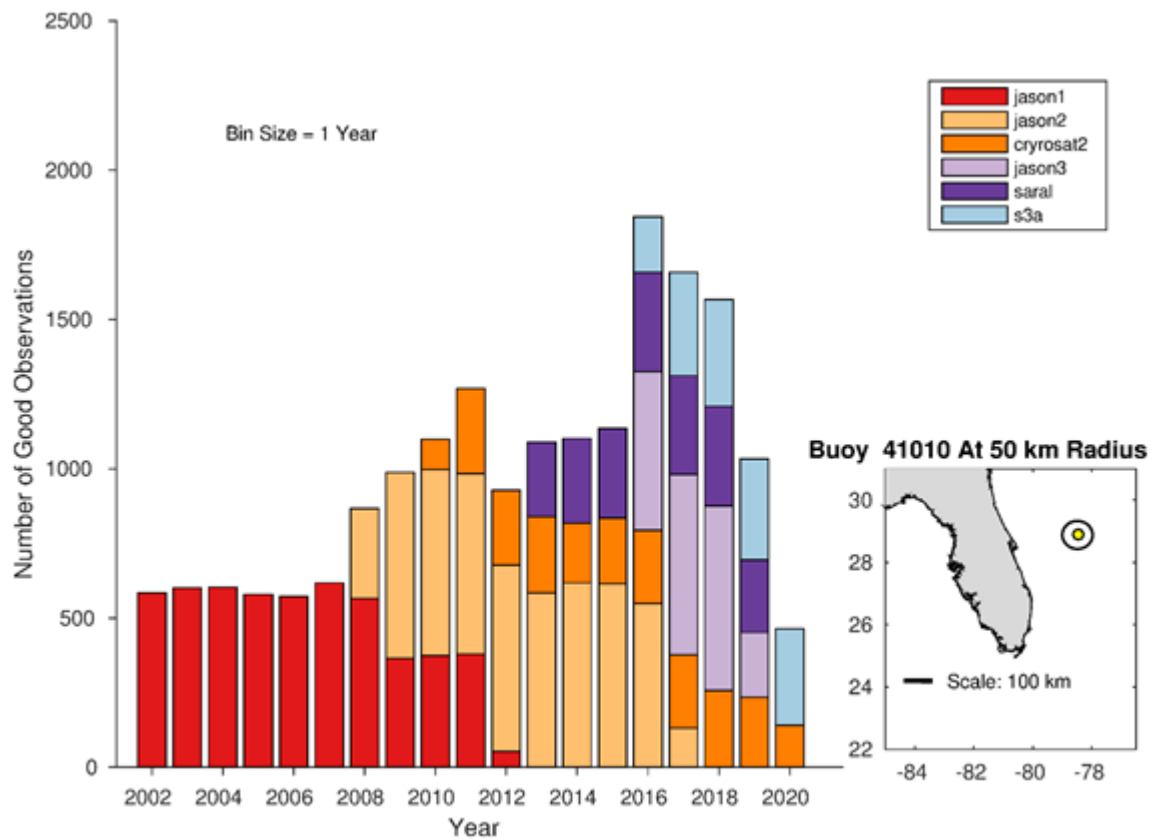


**Figure 2.1.3b** Temporal distribution (Jan 2002 to Dec 2020) of good observations (Quality Flag =3) of v2.06 and Sentinel 3A / SAR (v3) of the Sea State CCI multi- mission dataset at Buoy 41010.

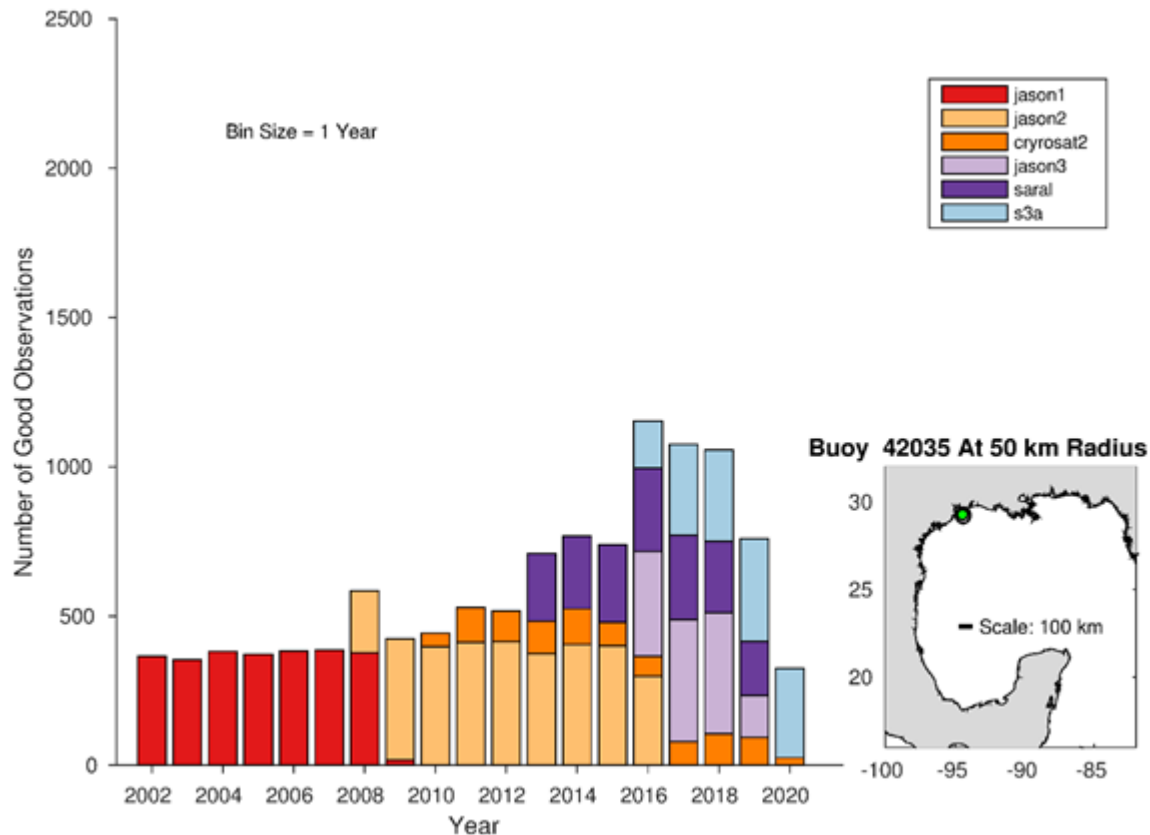


**Figure 2.1.3c** Temporal distribution (Jan 2002 to Dec 2020) of good observations (Quality Flag =3) of v2.06 and Sentinel 3A / SAR (v3) of the Sea State CCI multi- mission dataset at Buoy 42035.

### 2.1.6 Conclusions and Recommendations

We examined the suitability of Sea State CCI v2 products to study extremes at coast.

Sea State CCI v2 data are broadly consistent with v1, producing similar numbers of valid measurements, with marginally better performance in low sea state conditions, and slightly increased biases in high sea states. Over the same time period (2002-2018), the number of valid extreme values is similar in v2 and v1 . The improvements in low sea states are likely to benefit analyses closer to the coast.

Exact determination of Sea State CCI performance in high sea states is limited however by the small number of samples for  $H_s > 4\text{m}$ . The much shorter time period covered by CCI v2 (2002 - 2019) further limits the applicability of Sea State CCI products to study sea state extremes at the coast.

As pointed out by Timmermans *et al.* (2020), more data are needed before it will become possible to carry out extreme value analysis of sea state in coastal regions in a climate context based on satellite data records. It is recommended that future Sea State CCI products endeavour to incorporate data from earlier satellite altimeter missions to extend the time series and enable climate studies .

## 2.2. Case Study 2: storm events: extremes & swell

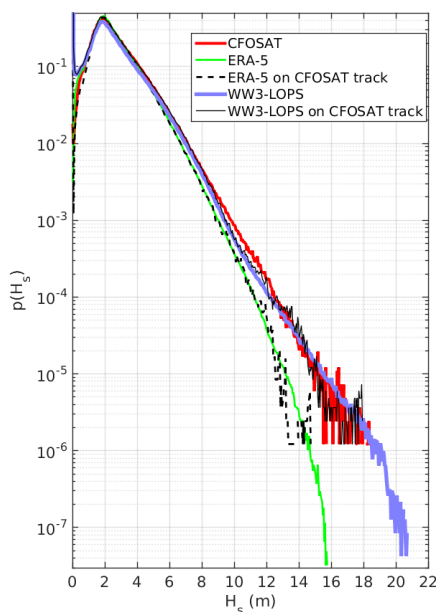
M. De Carlo & F. Ardhuin

Extreme sea states are important for the design of ocean and coastal structures, with 10 to 100 year return periods used for most applications, related to the lifetime of the object at sea. Extremes are also linked to strong upper ocean mixing and other geophysical applications. We also note that swell systems are fingerprints of the extreme ocean storms, and can propagate all the way across ocean basins from the area of high winds that generated them. Very long-period swells have been observed to propagate up to halfway around the globe (e.g. Munk et al., 1963). More recent investigations (e.g. Collard et al., 2009, Hannafin et al., 2011) clearly confirmed swell space-time persistence. Space-time analysis of ocean waves spectra measured from space at global scale can thus be used to monitor the same swell field over 3 to 10 days along their initial propagation direction.

### 2.2.1 Validation of extreme wave heights

Because of their large return periods, extremes are poorly sampled by satellites and in situ instruments, even if the highest wave heights generally correspond to storms that cover a very large area. As a result, the validation of extreme wave heights and estimation of uncertainties cannot rely on the straightforward application of the same kind of method used for more typical sea states, including the triple-collocation method (e.g. Abdalla et al. 2011). Given the measurement principle of altimeters, with a waveform related to the distribution of wave heights (Brown 1977, Passaro et al. 2014), it makes sense to extrapolate the validation and uncertainty estimates obtained for smaller wave heights. However, in the case of altimeters, it is also possible that the lower signal level associated with the larger mean square slopes and the stretching of the leading edge over a much wider range than usual may lead to particular errors that may be instrument dependent. For Synthetic Aperture Radar data, given the non-linear response of the SAR image to the sea state, it is not

impossible that errors in neural network estimates of wave parameters (Li et al. 2011) more strongly depend on wave heights outside of the range of the training data set. Also, the error also depends on the accuracy of the training data which is usually a modeled dataset.



We have thus chosen to look at statistical validation of the occurrence of extremes, using numerical models as a guide to assess the consistency of the wave height measurements. As shown on Fig. 2.2.1,

*Figure 2.2.1: Distribution of significant wave height for over the entire globe the full year 2019 from two different models (not corrected for larger area near the Equator), and co-located with CFOSAT nadir altimeter data.*

we have used waves from the ERA5 reanalysis (Hersbach et al. 2020) and from a non-assimilating wave model forced by ERA5 winds with an enhancement of wind speeds for winds stronger than 20 m/s, and a few other minor adjustments (Alday et al. 2021).

All distributions in Fig. 2.2.1 have almost no difference between 1 and 5 m, but deviate strongly for  $H_s > 8$  m. We note that the Alday et al. (2021) model is capable of producing  $H_s$  values above 16 m in 2019, which do not exist in ERA5. However, it is quite possible that the Alday et al. (2021) model overestimates the most extreme sea states.

Track by track inspection of the CFOSAT data suggest that there should be values up to 18 m in the North Atlantic. We note that this is the range of the maximum value of the 10 to 20 year return  $H_s$  for any given point in the North Atlantic (Vanem 2017). We have not attempted here to convert a maximum over an area to a local 10 year return period, or the expected maximum given satellite sampling. Instead the analysis presented here is closer to a quality check that is designed to answer the question: “Can we believe the very large values of SWH reported in the CCIV3 dataset, or is there something specific to warn the users against?”. As we show, this first analysis suggests that the values up to 20 m are plausible. This is summarized by Fig. 2.2.2.

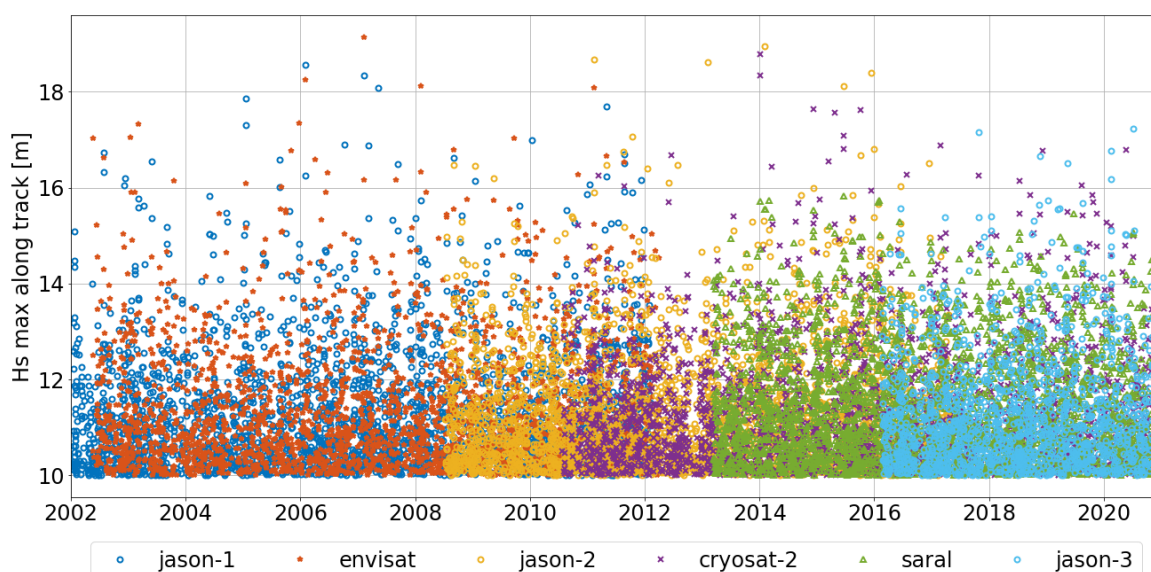


Figure 2.2.2: Maximum value for any half orbit that has a maximum 1 Hz (denoised) value above 10 m.

For each satellite track (half orbit data given by one CCIV3 file), the maximum value was checked and the track was further inspected if the maximum exceeded 10 m. For each of these tracks the data was co-located with model output and the shape of the peak was investigated. Fig. 2.2.2 also shows that SARAL  $swh\_denoised$  never exceeds 16 m, which appears very unlikely compared to the other missions for the same year. It is also important to note that  $H_s > 16$  m typically corresponds to a dozen or so storms every year, with a considerable year-on-year variability.

Fig. 2.2.3.a shows SARAL distributions of  $H_s$  for the years in common in the 3 CCI version datasets (2013–2018). The CCIV3 flags have been updated to remove the outliers above 20m that appeared in v2, and were not consistent with models (see Fig. 2.2.3.b). However, compared to CCIV1, there appears to be missing values for  $H_s$  above 14 m. These missing

values are also evidenced on Fig. 2.2.4 that shows distributions of  $H_s$  for 2018 in the CCIv1 and CCIv2 datasets. Compared to CCIv1, we also note a very strange shape of the  $H_s$  PDF in CCIv2 for  $H_s < 4$  m.

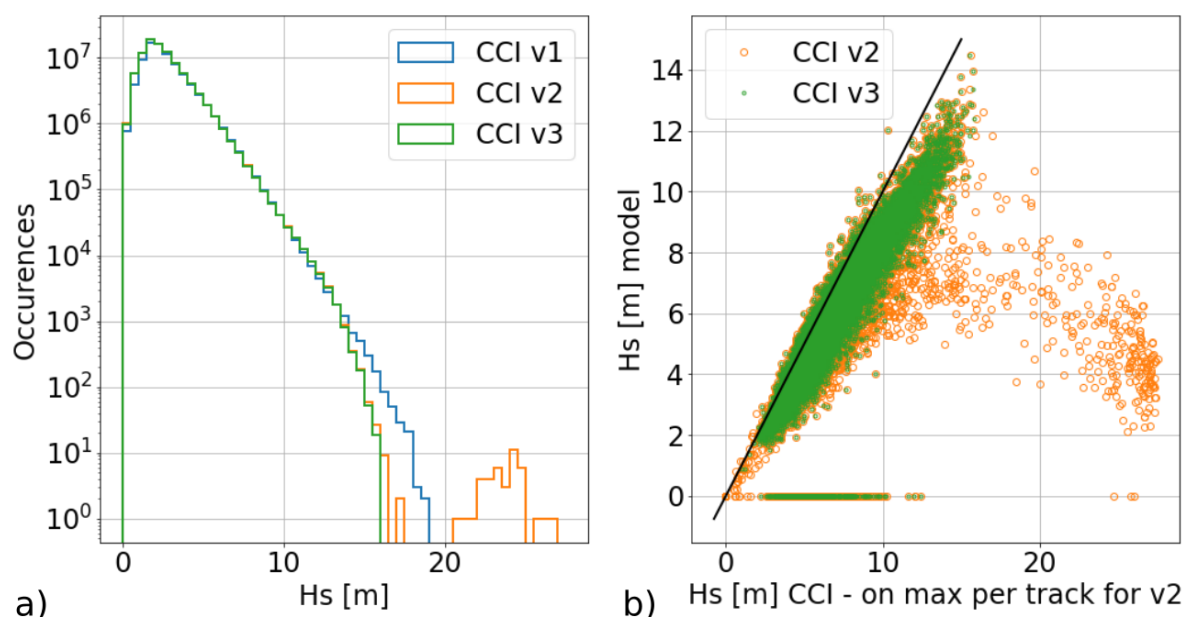


Figure 2.2.3.a Distribution of wave heights from SARAL from 2013 to 2018 in the CCIv1 (blue), CCIv2 (orange) and CCIv3 (green). b. Comparison of the maximum of  $H_s$  along CCIv2 half orbits and the wave heights extracted at the same point and time from the model and the CCIv3 dataset.

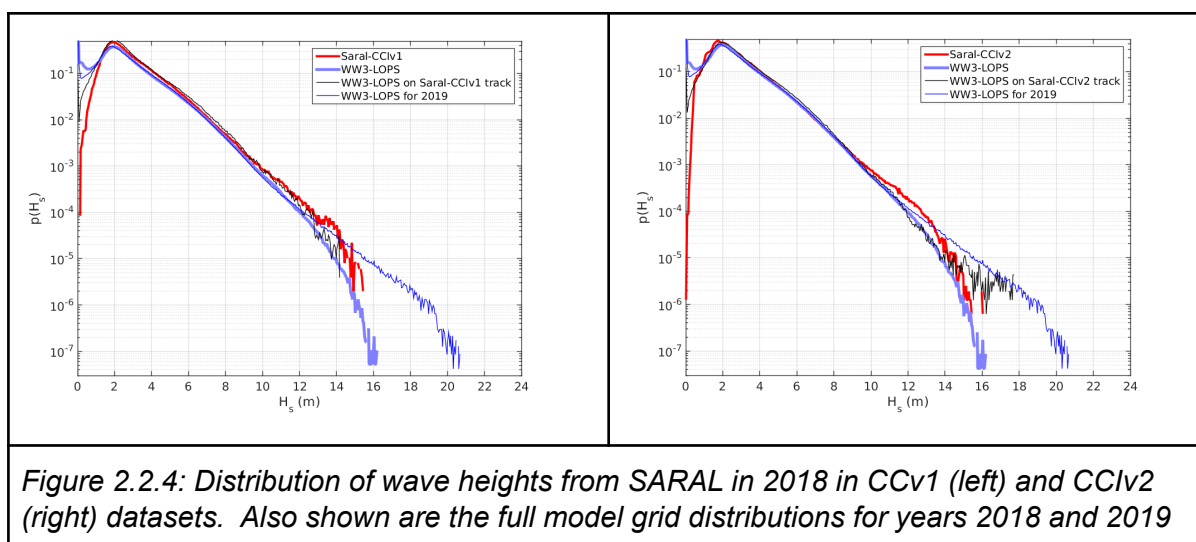


Figure 2.2.4: Distribution of wave heights from SARAL in 2018 in CCIv1 (left) and CCIv2 (right) datasets. Also shown are the full model grid distributions for years 2018 and 2019

The missing values above 14m seem to originate from higher RMS values in the CCIv2/3 than in the CCIv1, which in turn come from more scattered 40 Hz wave heights. Fig. 2.2.5 shows an example of a track with values above 14m for the CCIv1 dataset that are not present in the CCIv2 nor in the CCIv3 dataset.

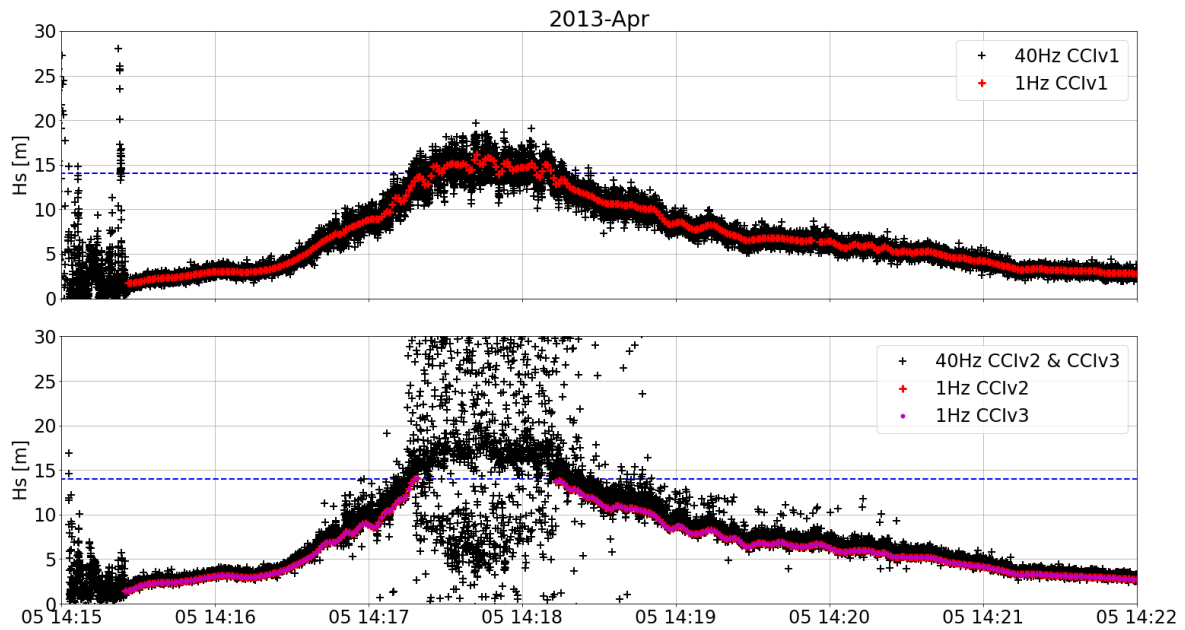
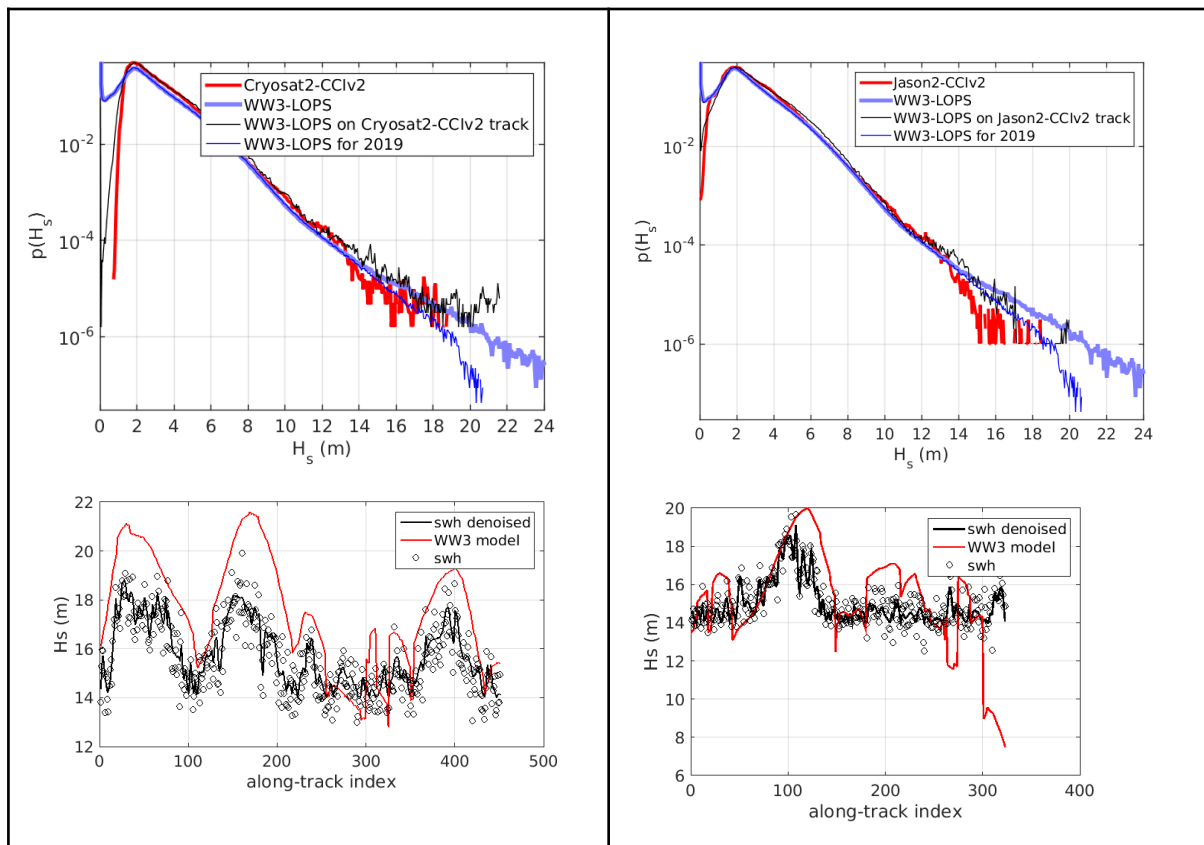
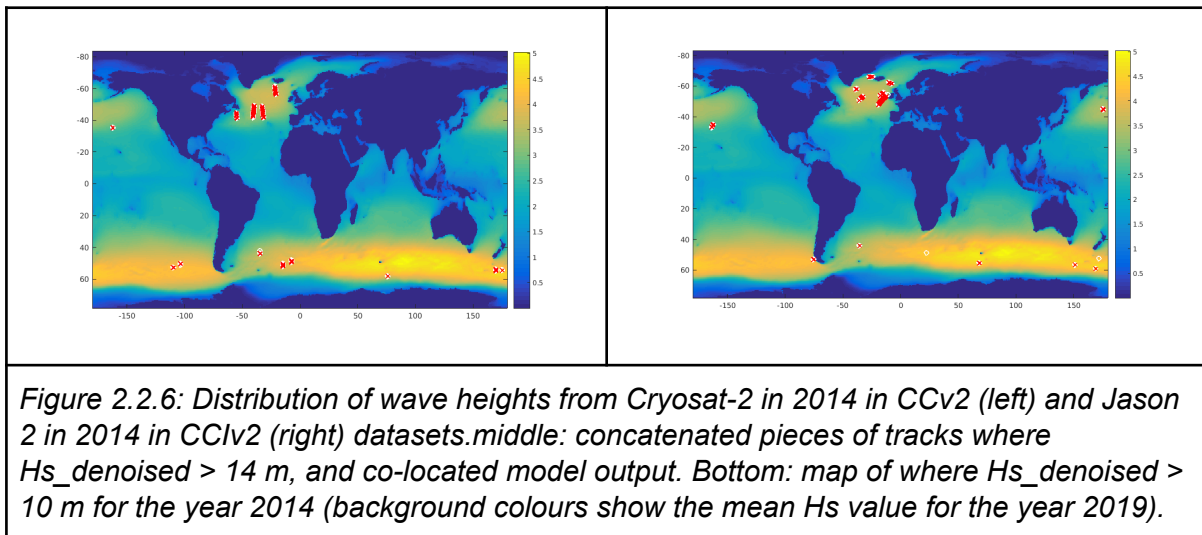


Figure 2.2.5 Significant wave height along a SARAL track, zoom over 7 minutes on April 5th 2013. Above: 40 Hz (black) and 1 Hz (red) values on the CCIv1 dataset. Below: 40 Hz (black) and 1 Hz values on the CCIv2 (red) and the CCIv3 (magenta) datasets. Blue dashed line is the  $H_s=14m$  limit.

The other missions processed in CCIv2 and CCIv3 have more “normal” distributions of the  $H_s$  values, with some examples in Fig. 2.2.6.







### 2.3. Case Study 3: Sea state decadal variability in the North Atlantic

A. Hochet & G. Dodet

Sea state is a key component of the coupling between the ocean and the atmosphere, the coasts and the sea ice. Understanding how sea state responds to the internal and external variability of the atmospheric circulation and how it affects the different compartments of the Earth System, is becoming more and more pressing in the context of increased greenhouse gas emission, accelerated sea level rise and sea ice melting, and growing coastline urbanization. Satellite altimeter missions have been recording wind and wave information continuously with a quasi-global coverage since the early 90s. This data has already proven very useful for investigating the decadal variability of wave heights and their link with the atmospheric circulation (Woolf et al., 2002; Young and Ribal, 2019). Recent studies have also revealed a global increase in wind speed (Hu et al., 2020) and wave power (Reguero et al., 2019). However, several factors make the interpretation of these findings difficult. First, the altimeter time records is of the same order as of the natural variability of the system depicted by multi-annual large-scale teleconnection patterns, such as the El Nino Southern Ocean oscillation, the North Atlantic Oscillation or the Pacific Decadal Oscillation, which makes it particularly tricky to extract the identification of any external contributions (Dodet et al., 2010; Hemer et al., 2010; Shimura et al., 2013, Stopa and Cheung, 2014). Second, the processing of heterogeneous altimeter data into a merged product is a complex task, which may lead to significant differences among different products generated from similar sources (Timmermans et al., 2020). For these reasons, computing robust long-term statistics from multi-mission altimeter products and separating underlying trend from the natural variability in historical  $Hs$  records still represent challenging topics.

In this case study, we use the Sea State CCI dataset that integrates improved altimeter retracking and inter-calibration methods in order to investigate the wave climate variability in the North Atlantic at multi-decadal scale. For a thorough review of the existing literature on sea state decadal variability in the North Atlantic, with some applications of the Sea State CCI dataset, please refer to Hochet et al. (2021).

### 2.3.1. Hs climatology

The sea state climatology in the NA has been described in many studies, using observations from satellites (Woolf et al., 2002), voluntary observing ships (Gulev and Grigorieva, 2006) or model reanalysis (Semedo et al., 2011). Here, we summarize the main characteristics of this variability using the Sea State CCI dataset v1 (L4 product) over the period 1993-2018. The time mean of Hs, computed for each calendar month over the period 1993-2018 is shown on Figure 2.2.6. The largest values, around 6 m, are found at high latitudes (between 40-60°N), in the central part of the basin bordered by the Labrador Sea, the Norwegian Sea and the Celtic Sea and for winter months from December to March. During summer months, the largest values of Hs are still located in the same region south of Greenland but have much smaller values with maximums around 3 m. This climatology of monthly mean Hs is in agreement with the one obtained by Woolf et al. (2002) with satellite data on a shorter period of time (1991-2000).

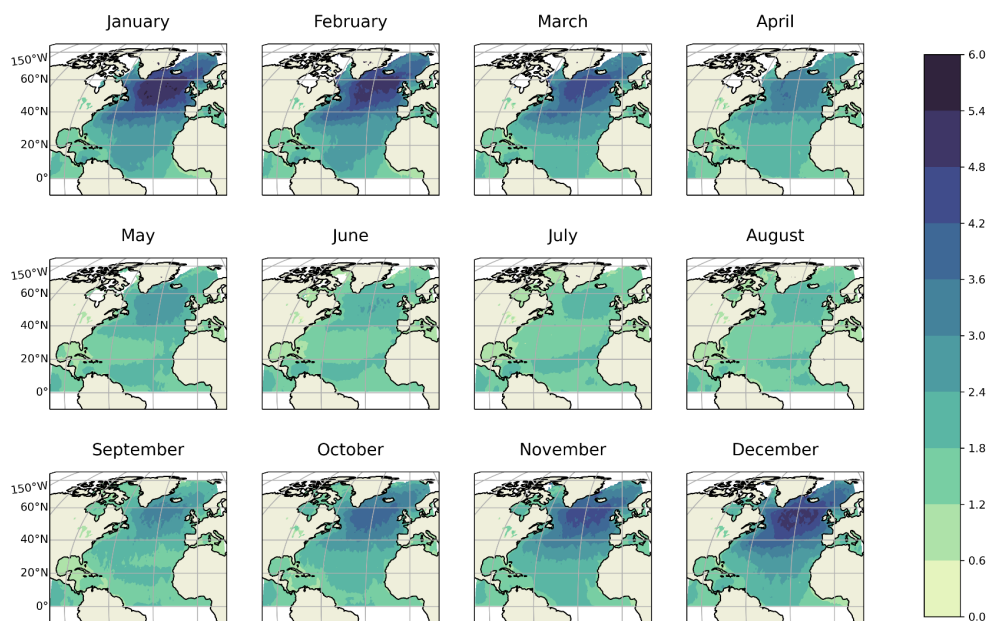


Figure 2.2.6. Maps of monthly mean of Hs (m) calculated over the period 1993-2018 using altimeter data.

Figure 2.2.7. shows the inter-annual variability of Hs, represented as the standard deviation computed on Hs for each month over the 1993-2019 period. The largest inter-annual variability is located in a region centered off the coast of Ireland, during the winter months (mainly November, December, January and February) with values up to 1.4 m in February. The inter-annual variability is much weaker at low latitudes ( $< 20^{\circ} \text{N}$ ) for all months. We can also note an increased Hs variability along the southern US Atlantic coast during the months of August and September, which may be related to tropical cyclone activity.

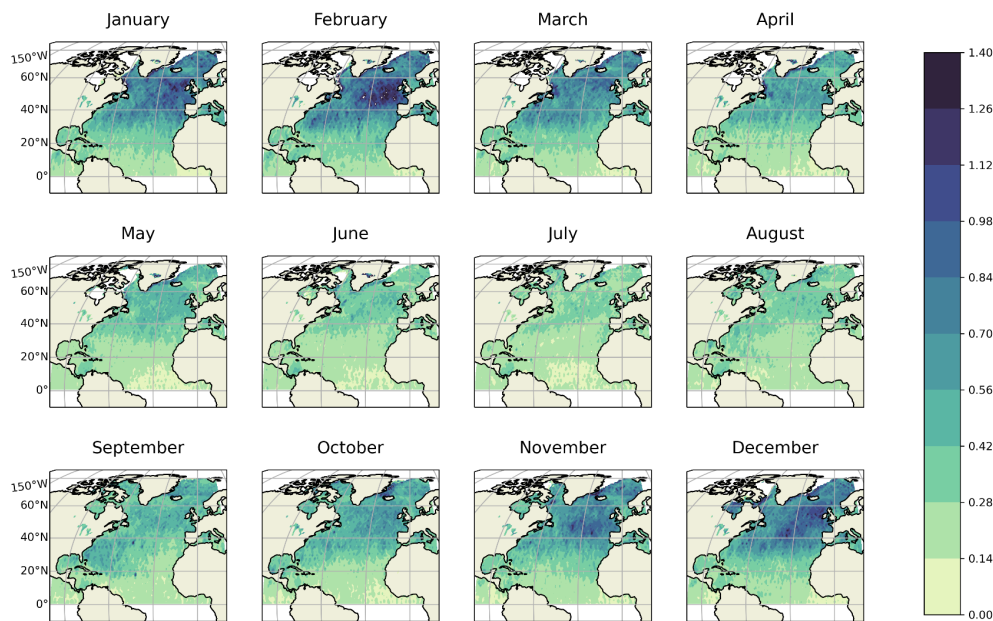


Figure 2.2.7. Standard deviation of  $H_s$  (m) obtained from each individual month over the period 1993-2018 using altimeter data.

Given the much stronger inter-annual variability of  $H_s$  observed during the winter months, the following analysis of the interactions between sea state and atmospheric circulation is focusing on winter (JFM) average statistics.

### 2.3.2. Comparison of NA SLP, NA wind intensity, climate modes as sea state predictors

To improve our understanding of the link between winter  $H_s$  and winter surface atmospheric fields, we investigate in this section the link between  $H_s$  and various climate modes selected for their known influence on  $H_s$  winter climate. Then, we test if the representation of winter  $H_s$  variability in the NA by these modes can be improved with the use of indices constructed from the Principal Components of either NA SLP or NA wind intensity. In order to have access to longer time-series than the one covered by satellite altimetry, we use the ERA 5 model reanalysis over the period 1980-2018.

The first two panels in Fig. 2.12 shows the 5% significant correlation level between the JFM average of  $H_s$  (obtained from ERA-5) and the NAO and EA indices which are known to be the main drivers of winter  $H_s$  inter-annual variability in the NA (Woolf et al. 2002). Consistent with previous studies using different datasets, correlations of winter  $H_s$  and winter NAO form a dipole with positive values in the North-Eastern Atlantic, off the coasts of the British Isles and negative values at latitudes around 35N, off the U.S. Positive significant correlations between winter  $H_s$  and winter EA are located off the coast of continental Europe and negative correlations are found at higher latitudes in the Norwegian Sea (not visible).

Proceeding with the same idea, we show in the remainder of Fig. 2.3.1. the time correlations of winter  $H_s$  and the winter average of 7 other climate modes (the list is given in figure) selected because they are known to have an effect on winter  $H_s$  variability (see for instance Shimura et al. 2013).

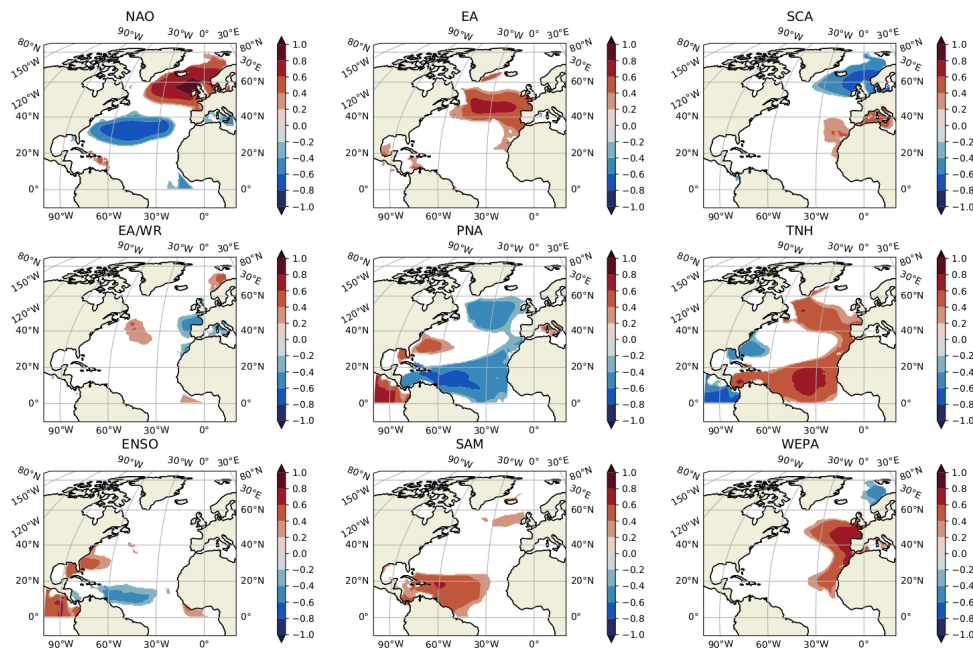


Figure 2.3.1: Time correlation between ERA-5 JFM Hs and the climate indices (1980-2018). Only 5% significant values are shown. From top to bottom, left to right correlations between Hs and the following indices are shown: NAO, EA, Scandinavian Pattern (SCA), East Atlantic /West Russia pattern (EAWR), Pacific-North American pattern (PNA), Tropical North Hemisphere pattern (TNH), El Niño-Southern Oscillation ENSO, Southern Annular Mode SAM and West Europe Pressure Anomaly (WEPA).

To better understand what part of JFM Hs variance is explained by the contribution of all climate modes considered here, a multivariate linear regression is used to regress Hs with the sum of all modes plus a linear trend as follows:

$$H_s(x, y, t) = \sum_{i=1}^9 \alpha_i(x, y) index_i(t) + \alpha(x, y)t + \beta(x, y) + \epsilon(x, y) \quad (1)$$

where  $\alpha_i$  are the coefficient given by the multivariate linear regression for  $index_i$ , which is one of the 9 indices studied here (i.e. NAO, EA, SCA, EAWR, PNA, TNH, ENSO, SAM and WEPA). At each location  $(x, y)$ ,  $index_i(t)$  is used only if its correlation with  $H_s(x, y, t)$  is significant.  $\alpha$  is the coefficient of the linear trend,  $\beta$  the intercept and  $\epsilon$  the error. The coefficient of determination  $R^2(x, y)$ , which is the ratio of the variance explained by the model over the total variance of Hs is shown in Figure 2.3.2. High values of  $R^2$  which indicate that the sum of the modes explain most of the Hs variance, are found off the coast of Western Europe and along the coast of Morocco, in a latitudinal band around 35N and in the western half of the basin at low latitudes. Low values of  $R^2$ , associated with low levels of explained Hs variance, are found in the eastern half of the basin at low latitudes, in the Gulf of Mexico, in a latitudinal band north of 20N, East of U.K., along the North-Eastern coast of North America and in the South-West of Greenland.

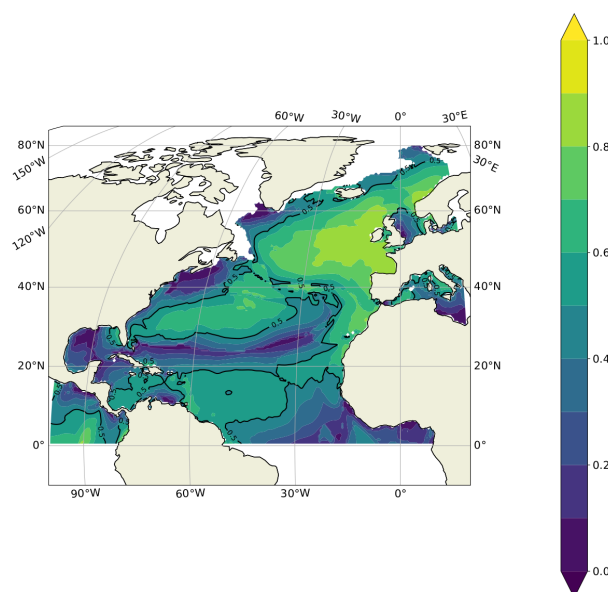


Figure 2.3.2: Coefficient of determination ( $R^2$ ) of all climate modes (i.e. NAO, EA, SCA, EA/WR, PNA, TNH, ENSO, SAM and WEPA) significantly correlated with JFM Hs. Values close to 1 (to 0) indicate that the JFM Hs variance is well (poorly) explained by the sum of the studied climate modes. The black contour line shows the 0.5 isocontour.

To test whether the amount of Hs variance explained by the contribution of the climate modes can be improved, we compute the PC of the EOF decomposition of winter SLP over the NA. Only the first 10 modes are retained as they explain more than 90% of the NA winter SLP variance. These PCs are then used as the new indices. Using the same method as for the climate modes described by equation (Eq.1), a multivariate regression of Hs on the PCs is computed and the corresponding coefficient of determination is shown on the left panel of figure 2.3.3. The right panel shows the coefficients of determination obtained with wind intensity over NA instead of SLP.

SLP over the NA explains an amount of Hs variability similar to that explained by the climate modes except at low latitudes, in the western half of the NA where the NA SLP has lower skills. These better results are due to a combination of PNA, TNH, ENSO and SAM which all display significant correlations with winter Hs. The wind intensity explains more Hs variability than NA SLP or the climate modes almost everywhere. The skill is particularly higher in the band of latitude just above 20 N where NA SLP and the climate modes have low skill.

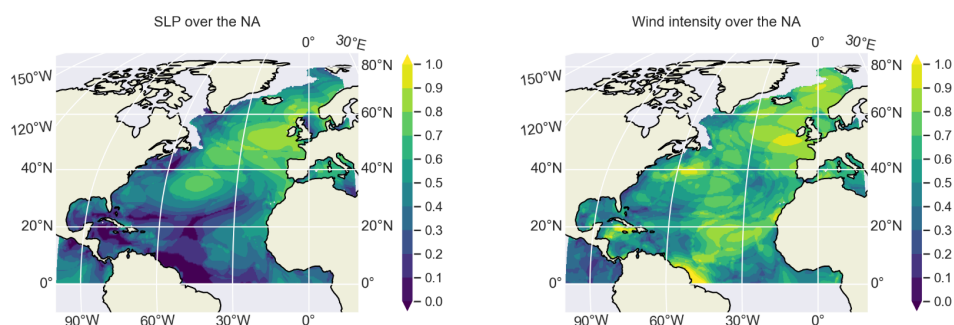


Figure 2.3.3 Same as Figure 2.3.2 but for the NA SLP (left) and wind intensity over NA (right).

### 2.3.3. Influence of NAO and EA on Hs trends

A number of studies have investigated Hs trends in the North Atlantic from in situ buoys (e.g. Komar and Allan, 2008), Voluntary Observing Ship data (e.g. Gulev and Hasse, 1999), or model reanalysis (e.g. Semedo et al., 2011) over different time periods. Key finding of these studies is that over decadal time periods the Hs variability is mostly controlled by climate oscillations and that the computed (linear) trends mostly reflect the phasing of Hs with these climate oscillations. Moreover, the climate oscillations that mostly drive Hs variability in the North Atlantic are the North Atlantic Oscillation (NAO) and the East Atlantic (EA) pattern, which are generally computed as the Principal Components of the first and second modes resulting from an EOF decomposition of the atmospheric pressure fields.

Figure 2.3.4 shows time-series of the winter (JFM) average NAO and EA indices computed from the monthly statistics provided by NOAA (<https://www.cpc.ncep.noaa.gov/>). Over the 1950-2020 time period, the winter NAO and EA indices both present distinct phases, with lower-than-average values between the 1950s and the 1980s, and higher-than-average values from the 1990s on, which result in statistically significant (at 95% level) positive trends over the whole period. Focusing on the uninterrupted altimetry era period 1993-2020, no statistically significant trends of NAO or EA indices are found.

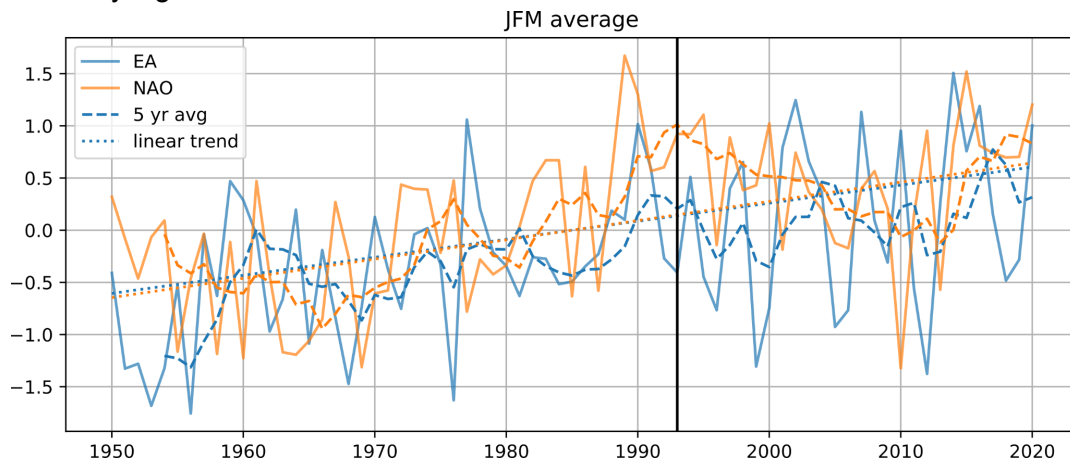


Figure 2.3.4. NOAA NAO and EA indices since 1950. No significant trends (at 95% level) in NAO and EA are detected over 1993-2018, while statistically significant positive trends are found over 1950-2020.

Hs trends can be computed from a simple linear regression as

$$Hs(x,y,t) = a_0(x,y)t + b_0(x,y) + R_0(x,y,t) \quad (2)$$

With  $a_0$  the slope term,  $b_0$  the intercept and  $R_0$  the residual. Figure 2.3.5. shows the Hs JFM trends computed in the NA from the Sea State CCI dataset v1 over the period 1993-2018. Negative values, down to  $-4 \text{ cm.yr}^{-1}$ , are found in the Norwegian sea and are statistically significant at the 5% level. Also, strong positive trends of Hs, up to  $4 \text{ cm yr}^{-1}$ , and statistically significant at the 5% level are found in the western part of the Mediterranean sea. Some significant positive trends of lower magnitudes (from  $1\text{-}2 \text{ cm.year}^{-1}$ ) are also observed along the eastern U.S. coast, the Caribbean Sea and in the tropical Atlantic.

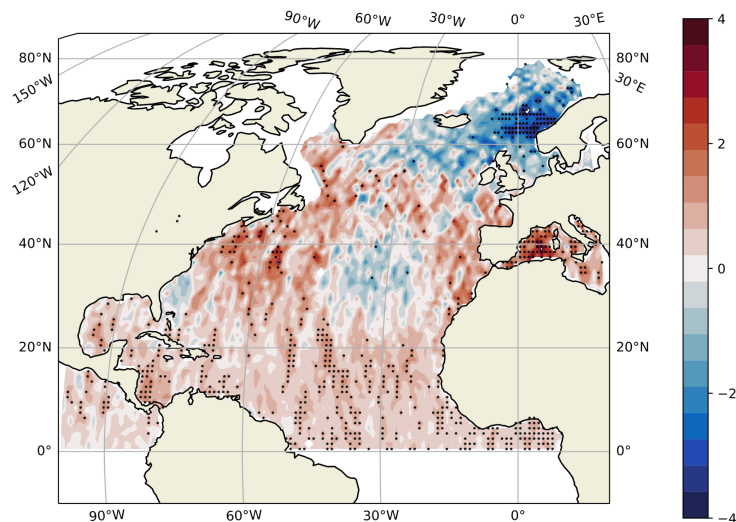


Figure 2.3.5. JFM trends (in  $\text{cm.yr}^{-1}$ ) of  $H_s$  computed on Sea State CCI dataset v1 for the period 1993-2018 ( $a_0$  in Eq.2). Dots indicate grid cells where the trend coefficient is significant at the 5% level.

This map shows significant differences with the trends obtained by Young and Ribal (2019) who used a different multi-mission altimeter product, covering the period 1985-2018, and did not find any significant trends in the North Atlantic. These differences can be explained by the different time periods covered by the altimeter products, but also by the different calibration methods and reference datasets they have used, in comparison to the one developed within the Sea State CCI project. Indeed, Timmermans et al. (2020) compared the version 1 of the Sea State CCI dataset with three other high-quality global datasets (Ribal and Young, 2019, hereafter, RY2019; ERA5; and CY46R1) using a consistent methodology, and found significant regional differences in wave height climatologies and trends (see their Figure 3). Yet, the overall patterns and the most significant trends in the Norwegian Sea and in the Mediterranean Sea were observed in the four datasets.

In order to investigate the contribution of the NAO and EA climate oscillation to the 25-year trends derived from the Sea State CCI dataset v1, Hochet et al. (2021) used a multiple variable linear regression approach to decompose the  $H_s$  signal as follows:

$$H_s(x, y, t) = a(x, y)t + b(x, y) + c(x, y)NAO(t) + d(x, y)EA(t) + R(x, y, t) \quad (3)$$

where NAO and EA are the winter mean climate index time-series,  $a$  and  $b$  are the  $H_s$  linear trends coefficients obtained from the multiple linear regression,  $c$  and  $d$  are regressions with respect to NAO and EA respectively, and  $R$  is the residual term. Left panel of Figure 2.3.6. shows the JFM  $H_s$  trends when the contributions of the NAO and EA are accounted for in the total  $H_s$  trend signal, ie  $a$  in eq. 3 and right panel of Figure 2.18 shows the trend associated with NAO and EA, computed as  $a_0 - a$  (right panel). We see that the contributions of NAO and EA present positive values up to  $1 \text{ cm.year}^{-1}$  in the central part of the domain, but have only a minor influence on the trends derived from the total  $H_s$  signal in the North East Atlantic, suggesting that trends in NAO and EA do not fully explain the observed trends in this region over the period 1993-2018 .

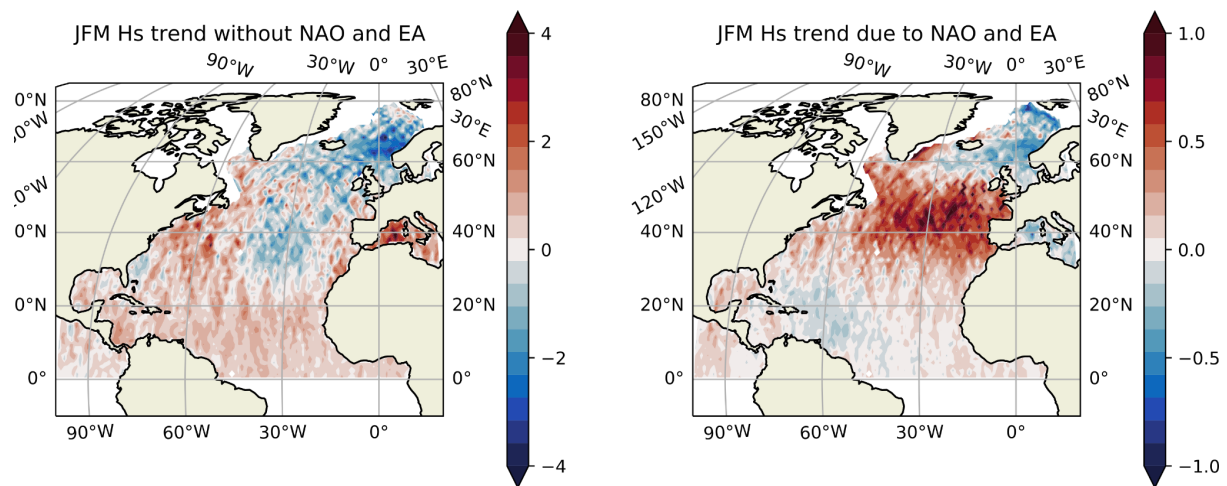


Figure 2.3.6: Left: JFM Hs trend (cm/yr) with NAO and EA influence removed (a in Eq. 2). Right: trends associated with NAO and EA (a-a0 in Eq. 1 and Eq. 2). Note the different colour scale between the two plots.

#### 2.4. Case Study 4: Waves in the marginal ice zone (NERSC)

The Case Study 4 consists of two parts. Part 1, “Impact of waves on marginal ice zone (MIZ) in 2015” discusses in detail the impact of waves as observed on along-track L3 data on the MIZ observed on individual Sentinel-1 SAR images. Part 2, “Wave climate in the Arctic and relation to MIZ width and ice extent” studies long term changes of significant wave height in the Arctic using L4 data and MIZ estimation from sea ice charts.

##### 2.4.1 Impact of waves on marginal ice zone (MIZ) in 2015

Waves penetrating into the pack break ice up into floes forming a region known as the marginal ice zone (MIZ). Simulations show (William et al., 2017) that while speed of ice edge retreat depends strongly on wind speed, the width of the MIZ depends solely on wave height and direction with sensitivity to small scale sea ice cohesion. Figure 2.4.1. shows dependence of MIZ width on wave period for (a) wind seas and (b) swells for strongly cohesive (multi-year) ice, moderately cohesive (first-year) ice and weakly cohesive (deformed pancake) ice.



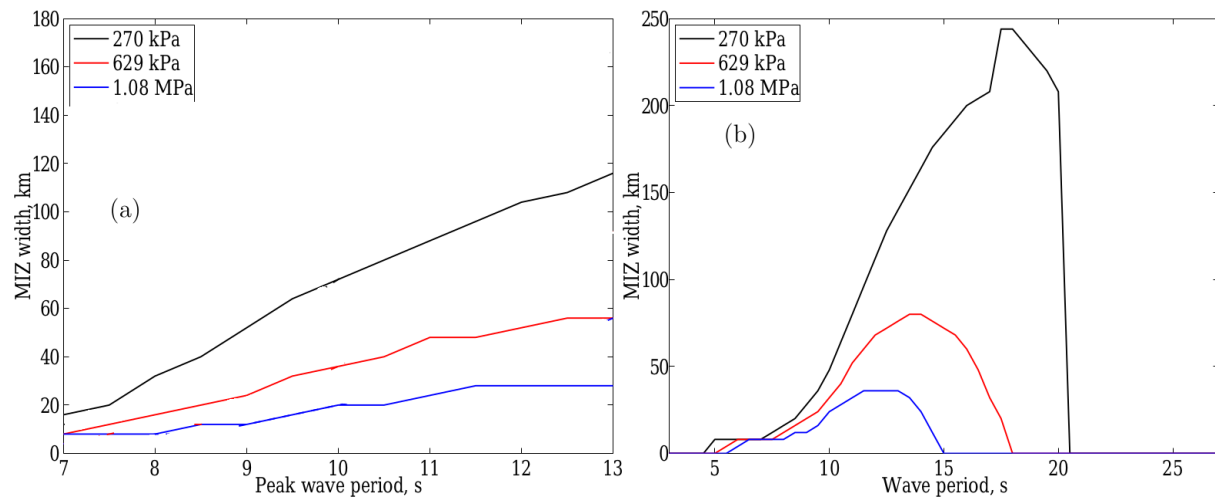


Figure 2.4.1: Variation of MIZ width with peak wave period and small-scale cohesion for (a) wind seas with significant wave height being 4 m and (b) swells with waves of height 3 m. For both plots, the concentration is 0.7, the thickness is 1 m.

MIZ and other ice types can be manually or automatically detected on SAR data from Sentinel-1, Radarsat-2, Envisat or other satellites (Zakhvatkina et al., 2017). Several operational institutes including MET Norway, Danish Meteorological Institute, Russian Arctic and Antarctic Research Institute (AARI) provide operational ice charting services for manual ice type classification based on various sources (fig. 2.4.2). Both original SAR data and operational ice charts are freely available either through different sources including Copernicus Environmental Marine Services.

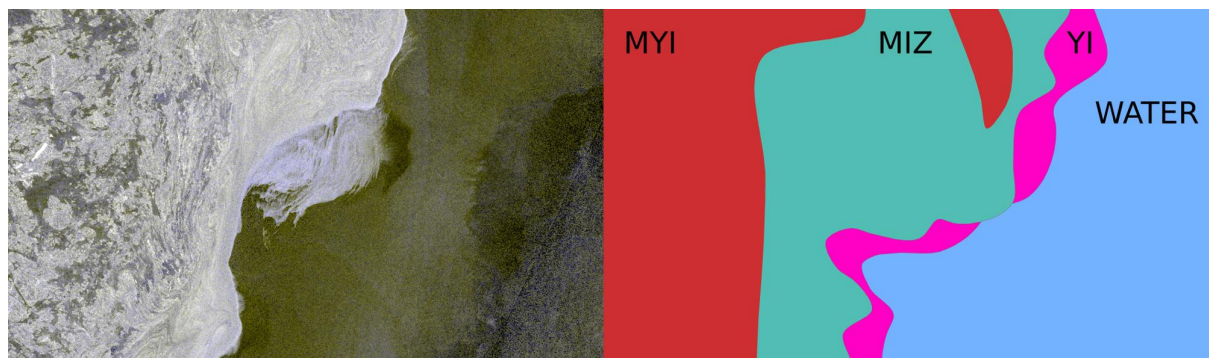


Figure 2.4.2: Comparison of Sentinel-1 SAR image with a manual ice chart from AARI (1 Jan 2017).

In the marginal ice zone, the observed sea state parameters provided in the CCI products are compared with the dynamics of the MIZ width estimated from sequences of SAR images or ice charts. The comparison is performed on a case by case basis for an identified extreme short term event. Long term changes and large scale anomalies (such as ice minima in 2007 and 2012) will be analyzed additionally.

The first use case included a study of a storm event in November 2015. The overall objective of this use case was to analyze the applicability of the data from the Sea State CCI project for studying the impact of waves on temporal variability of marginal ice zone (MIZ) in the Fram Strait. The data used for this study included:

- A mosaic of 11 Sentinel-1 SAR images acquired over the Fram Strait in the period from 22 November to 2 December 2015;
- Values of significant wave height (SWH) from the the ESACCI-SEASTATE-L3-SWH-MULTI\_1D product averaged over the region of interest on daily basis;
- Outputs from the WAVEWATCH III (WW3) model available on the Copernicus Marine Environmental Monitoring Service (CMEMS).

Figure 2.4.3. shows an example mosaic of Sentinel-1 SAR images taken over the region of interest on 22 November 2015. The marginal ice zone is visible as a stripe of ice with high backscatter and high homogeneity at the interface of pack ice and open water. In the beginning of the event MIZ is very narrow and extends into the open ocean in forms of filaments. Ice concentration in the pack is relatively low - a lot of leads crossing the ice pack can be observed. These conditions correspond to low waves conditions (SWH < 2 m) as also simulated by the WW3 model (see figure 2.4.4).

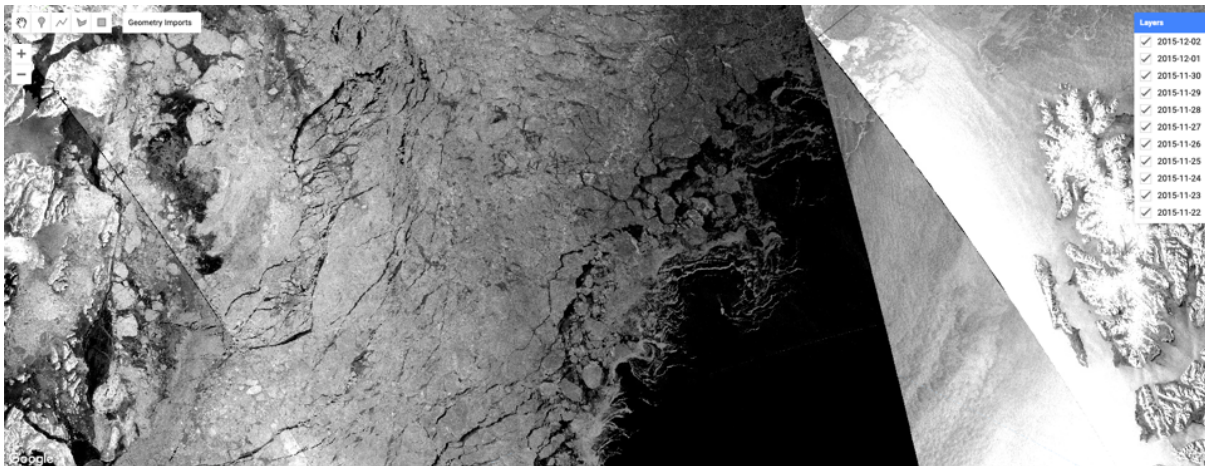


Figure 2.4.3. Mosaic of Sentinel-1 SAR images in HV polarization taken over the region of interest on 22 Nov 2015.

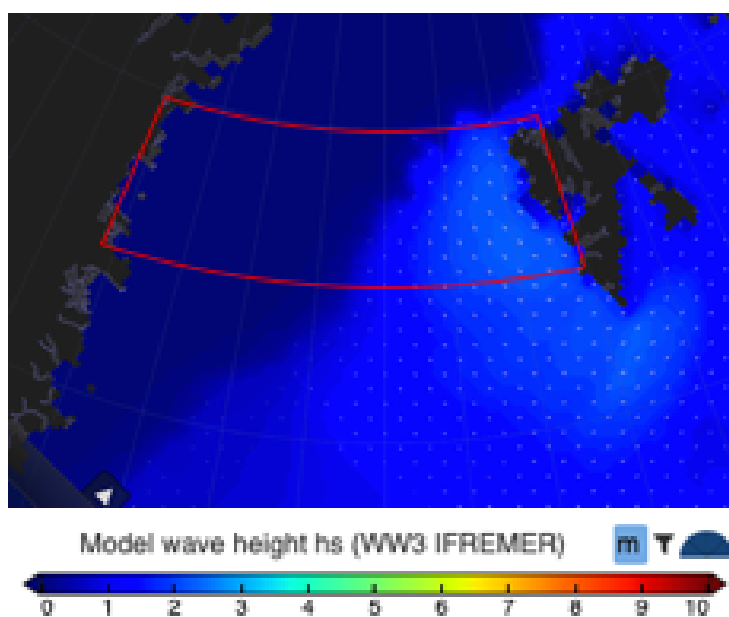


Figure 2.4.4. Output from WW3 model for 22 Nov 2015. Outline of the region of interest is shown by the red line. Colors correspond to the model wave height.

In the middle of the event on 28th November (shown on figure 2.4.5) the significant wave height predicted by the WW3 model is quite high (SWH > 6 m). The ice is compacted by wind and the concentration increases in the pack (see figure 2.4.6). MIZ width increases to 20 km and is clearly seen on SAR data.

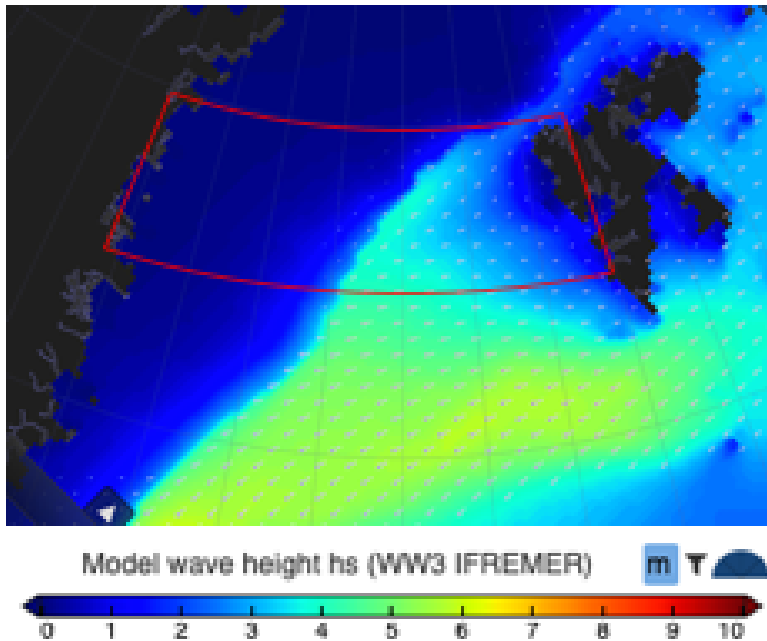


Figure 2.4.5. Output from WW3 model for 28 Nov 2015. Outline of the region of interest is shown by the red line. Colors correspond to the model wave height.

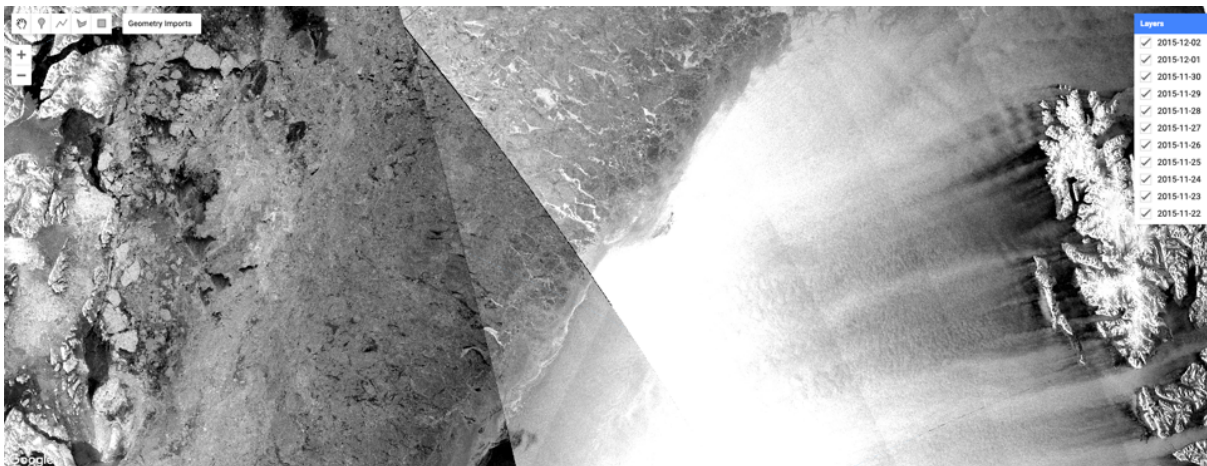


Figure 2.4.6. Mosaic of Sentinel-1 SAR images in HV polarization taken over the region of interest on 28 Nov 2015.

For these dates all available points from the ESACCI-SEASTATE-L3-SWH-MULTI\_1D product were collected as shown on figure 2.4.7 (left). Values of SWH were averaged on a daily basis and compared to the width of MIZ. Comparison, presented on figure 2.20 (right), shows that SWH increases from 1 - 2 meters to 5 - 6 meters in just a few days and this is followed by an increase of MIZ width up to 20 km with a 2 - 3 days lag. After the storm is gone SWH reduces back to 3 - 4 m and MIZ width decreases back to 10 - 15 km.

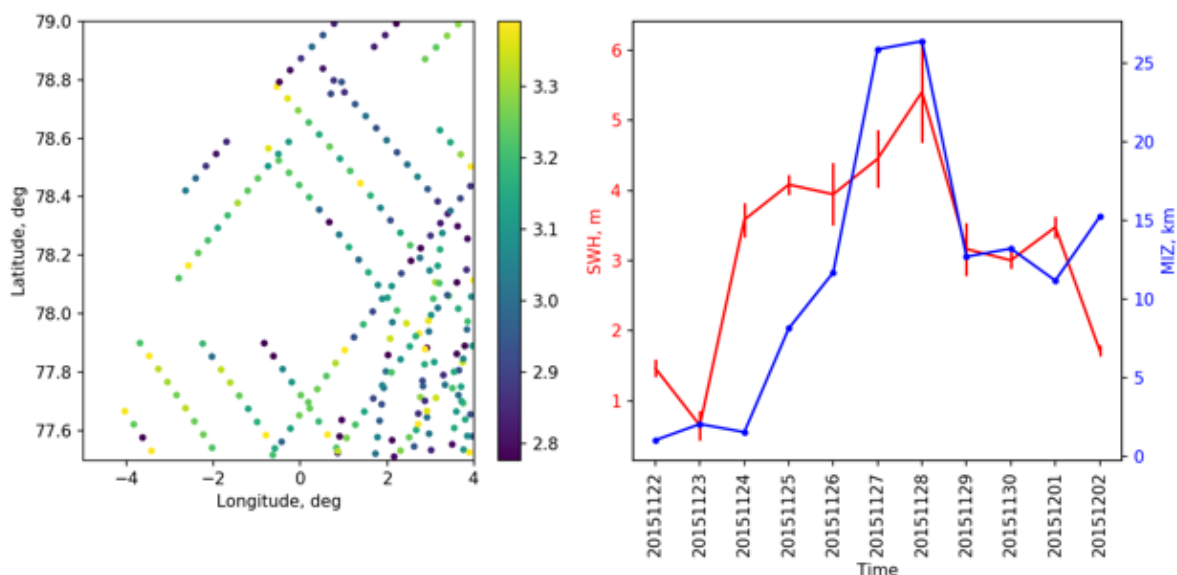


Figure 2.4.7. Left: Plot of all SWH points from the ESACCI-SEASTATE-L3-SWH-MULTI\_1D product covering the region of interest. Right: Comparison of SWH and MIZ width during the storm event.

This use case allows us to conclude that evolution of the ice edge position and MIZ width corresponds well to the timing of storms also observed on Sea State CCI L3 data. The identified relation is interesting for modelers for calibration / validation of waves-in-ice models. Detection of MIZ width should be automated and the approach extended to cover several years / regions. L3 data from the ESACCI-SEASTATE-L3-SWH-MULTI\_1D product is somewhat scarce in space and doesn't contain directional components which prevents a more detailed study and requires usage of WW3 model for better interpretation of results. L4 data is at monthly resolution and is not usable for studying high frequency (several days) changes in MIZ.

### 2.4.2 Wave climate in the Arctic in relation to marginal ice zone and sea ice extent

In this part of Use Case 4 we extend the study of waves climate in the Arctic [Stopa et al., 2016] by altimeter observations time series from 2002 to 2019. In addition, the significant wave height is compared to the width of the marginal ice zone (MIZ) retrieved from sea ice charts prepared by the National Ice Center (US) in the Chukchi sea in 2005 - 2016.

In our study we used the monthly L4 product ESACCI-SEASTATE-L4-SWH-MULTI\_1M, v2.0.6. It is a gridded product generated by optimal interpolation along-track Hs measurements by altimeters. The following variables from the product were used in the analysis: `swh_mean`, `swh_max`, `swh_squared_sum`, `swh_log_sum`, `swh_log_squared_sum`, `swh_count_greater_than_2.00` and `swh_count_greater_than_4.00`. The variable `swh_count` was used to normalize the squared or logged sums or the counts. The L4 gridded products were reprojected on the grid in Polar Stereographic projection with central longitude at 180° E, with resolution of 4 km and with the extent  $-2.5 \cdot 10^6 - 2.5 \cdot 10^6$  m northing,  $-2.5 \cdot 10^6 - 2.5 \cdot 10^6$  m easting.

Similar to the study of Stopa et al., [2016] we averaged Hs for winter (January, February, March) and summer (August, September, October) seasons and computed trends over the entire period of the L4 product: 2002 - 2019 (see Fig. 2.4.8). Deseasonalized trends were computed

using Sen's method with Mann-Kendall test for significance [Hussain, 2019] in regions where data spans at least 10 years.

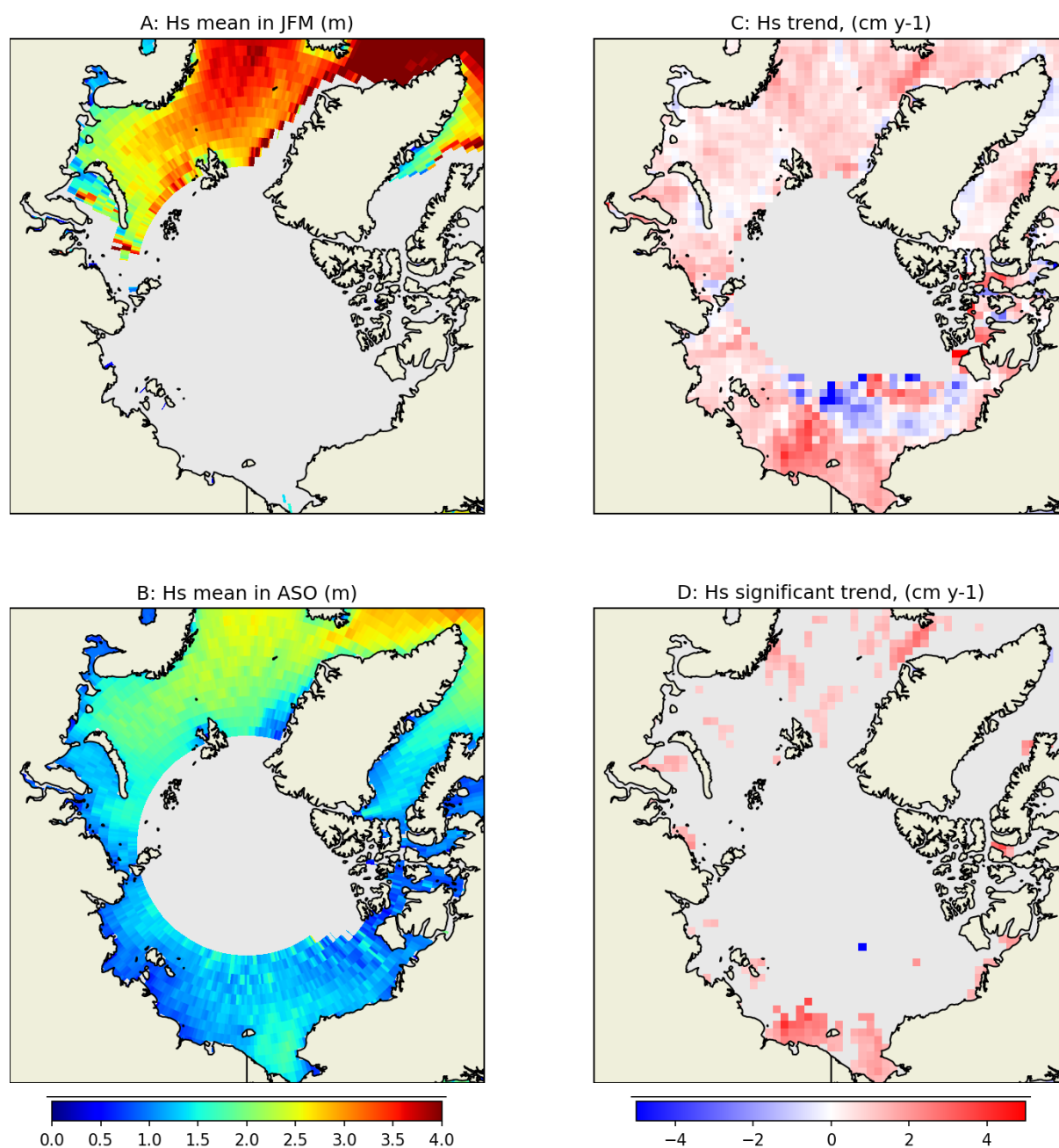


Figure 2.4.8. Averaged significant wave height and trends in the Arctic. A: Mean Hs in winter period (January, February, March). B: Mean Hs in the Arctic in summer period (August, September, October). C: Trends in monthly averaged Hs in all regions. D: Trends in monthly averaged Hs in regions with sufficient significance.

Similar to the results in [Stopa et al., 2016] in winter the maximum Hs (3.5 - 4 m) is observed in the North Atlantic with a gradual decay towards the Barents Sea (2 - 2.5 m) and the Kara Sea (1.5 - 2 m). A seemingly artificial jump of Hs up to 5 m is observed in the Greenland Sea, south of 66°N. In the summer season, the extent of data coverage is larger due to low sea ice coverage and the Hs values are lower: ~2.5 m in the North Atlantic, ~2m in the Barents Sea, ~ 1 m in the Kara Sea, < 1 m in the Russian Arctic seas and the Beaufort Sea,

~1.5 m in Chukchi Sea, 1.5 - 2 m and 2 - 3 m in Baffin Bay and Greenland Sea, correspondingly. Unfortunately, the SS CCI product doesn't extend further than 80°N.

The trends computed from the period 2002 - 2019 are somewhat different from the results in [Stopa et al., 2016] computed from period 1992 - 2014. For example, in the North Atlantic and the Barents Sea the trends are positive, although weak and mostly insignificant. In the Chukchi and East-Siberian seas the correspondence between the two studies is better - the trends are significant and positive. Interesting to note a small region with negative (although mostly insignificant) trends near the ice edge, well corresponding to Fig. 7 in [Stopa et al., 2016].

After detecting significant trends in Hs several regions of the Arctic it was attempted to find a relation with the sea ice extent and marginal ice zone. Sea ice concentration and MIZ was detected on the weekly sea ice charts produced by the U.S. National Ice Center (<https://usicecenter.gov/>). The ice charts are prepared by ice analysts and are provided as shapefiles with polygons describing sea ice state using WMO nomenclature. The weekly ice charts contain information on both sea ice concentration, sea ice stage of development and, in some areas, on sea ice form. Concentration can be used to estimate the extent of sea ice. Stage of development tells about the age of the ice in each polygon (e.g. nilas, young ice, first year ice, multi-year ice). Form of ice tells about floe size distribution and compactness of the ice field. In each polygon information about three ice types dominant in the polygon is presented. The ice charts were used under the assumption that the form of ice field can be used to identify MIZ. For this reason the polygons with floe size between 30 cm (pancake ice) and 500 m (medium floe) and in the vicinity of open water were considered as belonging to MIZ (see examples on Fig. 2.4.9). The vector ice charts were rasterized by GDAL on a similar grid as SWH but with the resolution of 2 km.

Unfortunately, it was found that the information on the form of ice is provided only in a few regions - along the Alaskan and Canadian coast in the Beaufort Sea and Chukchi Sea and in Baffin bay. The longest and the most consistent time series of the form of ice was found to be in the Chukchi Sea. There the time series span the period 2004 - 2015.

Figure 2.4.9. shows maps of Hs (swh\_mean product) and sea ice extent in the Chukchi and Beaufort Sea for an example summer season in 2006. It is clear that the suggested methodology in most cases quite successfully detects the MIZ. However in a few cases, e.g. June 26 or July 27 the MIZ erroneously extends too far from the actual ice margin. This seasonal time series doesn't allow to visually identify a relation between MIZ width and Hs - MIZ is the widest in August and early September and later in November, whereas the Hs is highest in October. One of the obvious reasons is low temporal resolution of the L4 SWH product. Therefore, the relation was studied at interannual time scales.

Only the region of interest outlined by a red box on Fig. 2.4.9 was considered for analysis as it represents a relatively homogeneous distribution of Hs and easily interpretable distribution of sea ice with small to medium floes. Whereas in the Russian Arctic the information on the form of ice was not presented, and in the Beaufort Sea the broken up ice is also observed inside the ice pack - far from the ice margin.

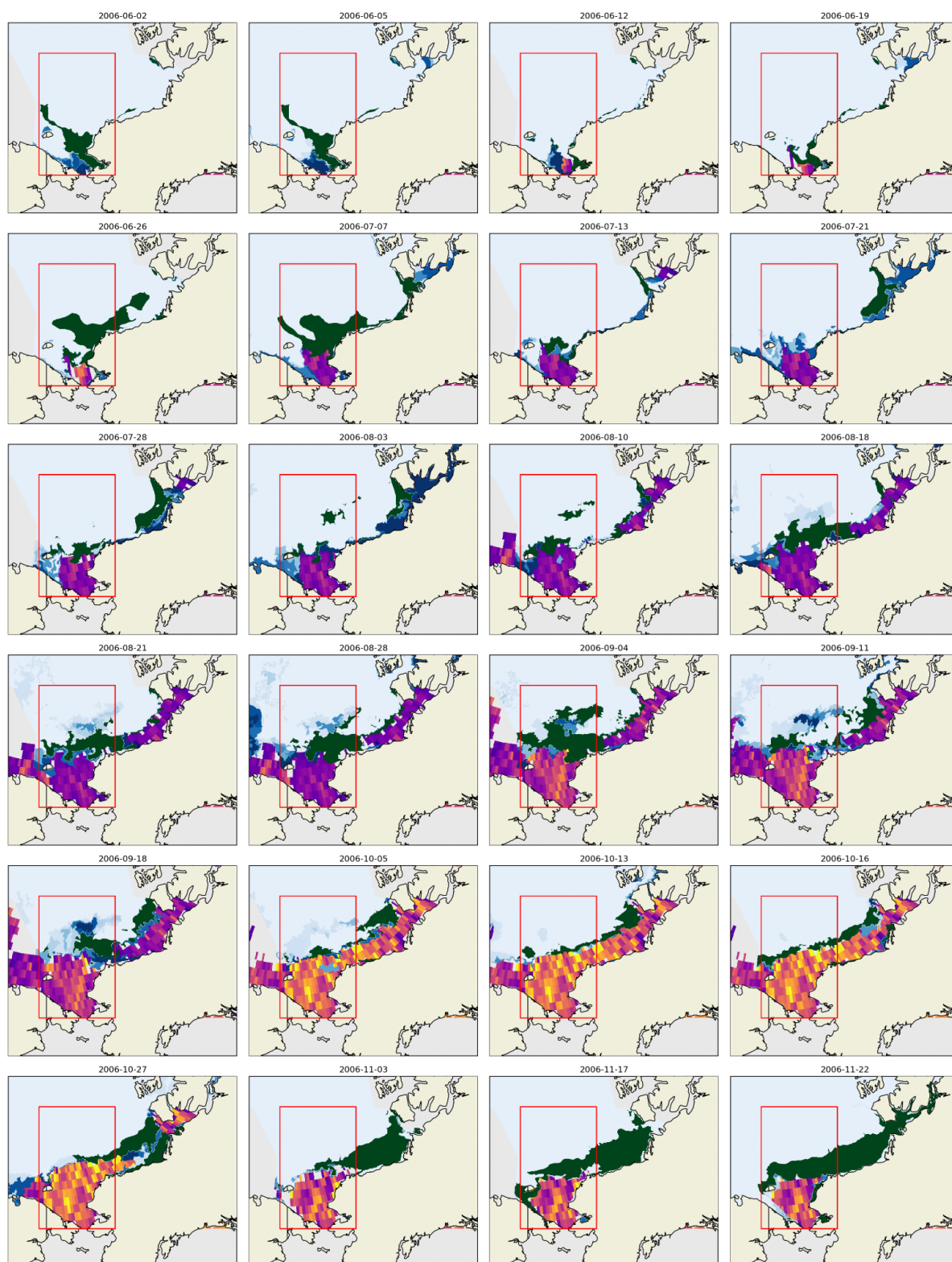


Figure 2.4.9. Series of weekly maps of the Chukchi sea, Bering strait and Beaufort sea for June - November 2006 showing sea ice concentration (shades of blue), extent of marginal ice zone detected by NIC experts (green color) and significant wave height from the SST CCI L4 product. Red box shows the region of interest.

For characterizing sea ice and MIZ numerically, the total area of sea ice and area of pixels detected as MIZ inside the region of interest was computed. At the same time  $H_s$  was averaged over the valid pixels inside the region of interest. Time series of all variables with

Hs from the L4 products were computed (i.e., swh\_mean, swh\_max, swh\_squared\_sum, etc). Figure 2.4.10. shows the time series of ice, MIZ and Hs (swh\_mean and swh\_max) for the period when both SWH and ice data were available. In winter months sea ice area caps at  $\sim 1.3\text{M km}^2$  because the entire region of interest is filled by ice. At the same winter periods wave observations are not available. In summer months sea ice concentration decreases and Hs shows a tendency to increase from the beginning of the season in June to the end of season in November. MIZ doesn't show a clear and persistent seasonal tendency but usually low MIZ areas correspond to low areas of the total sea ice cover. An obvious interannual variability in both ice and waves characteristics is observable but the relation between them cannot be deduced easily.

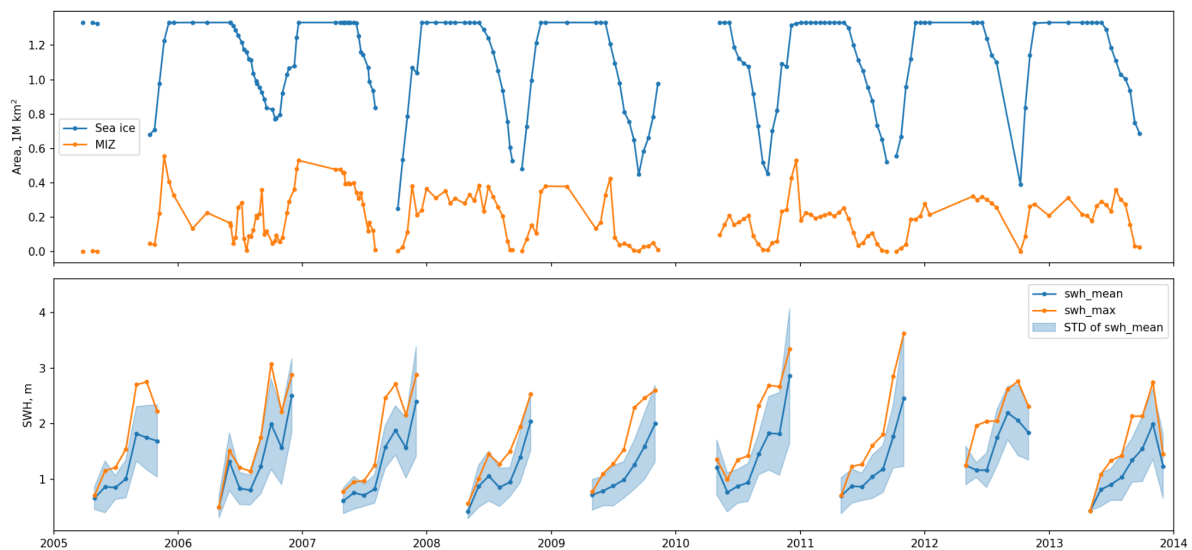


Figure 2.4.10. Time series of total sea ice area (blue) and MIZ area (orange) in the region of interest at weekly time step (upper plot) and significant wave height averaged over the region of interest (lower plot). Two Hs quantities from the L4 product are shown: swh\_mean (blue) and swh\_max (orange) with blue filling shown standard deviations from spatial averaging of swh\_mean.

Identification of relation between Hs and ice parameters (total ice area and MIZ area) was performed by correlation analysis of the time series coinciding in time. All Hs variables were tested in that analysis. Other statistical characteristics were computed from Hs spatial distributions in addition to averaging over the region of interest: maximum value, P90, standard deviation. Relation was tried to be found in several months separately (from June to November) or joined in seasons (e.g. June-July, August-September, October-November, or other combinations). The boundaries of the region of interest were also varied slightly to test the effect on the significance of the found correlations.

These experiments showed that only the relation of swh\_mean and swh\_max with MIZ area and ice area could be found for month June, July and August-September as shown on Fig. 2.4.11.



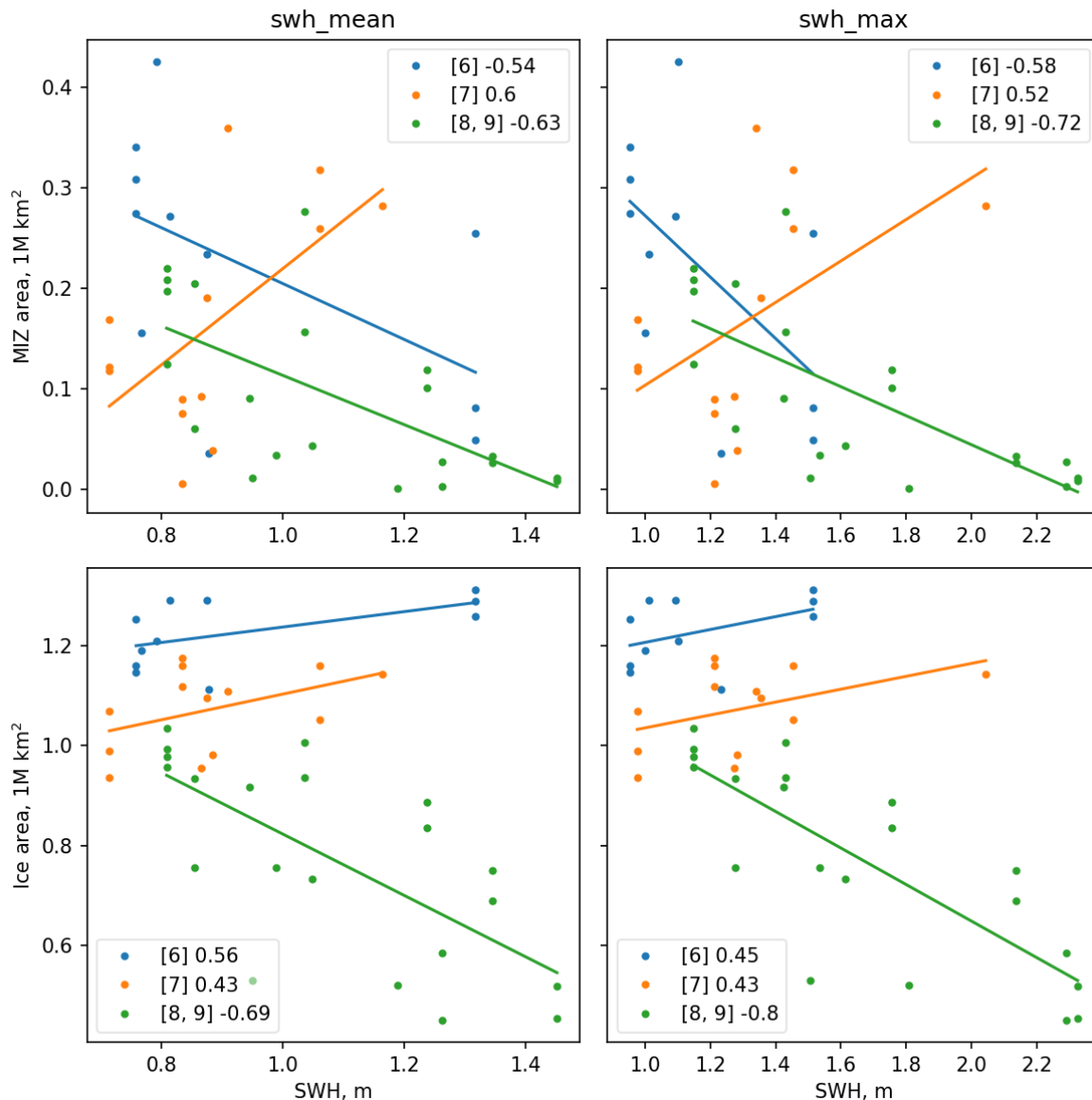


Figure 2.4.11. Scatterplots comparing `swh_mean` (X-axis, left column) and `swh_max` (X-axis, right column) with MIZ area (Y-axis, upper row) and total ice area (Y-axis, lower row). Colors denote three different seasons: blue - June, orange - July, green - August and September. Numbers on the legend show Pearson's correlation coefficient.

The following interpretation of the observed relations can be suggested.

In June mean and max Hs is inversely proportional to the MIZ area ( $r = -0.54$  and  $-0.58$ ) and proportional to the ice area ( $r = 0.56$  and  $0.45$ ) with moderate number of observations ( $N=11$ ). Probably, colder years with stronger winds and waves correspond to larger ice extent and thicker and stronger ice. The fetch in June is still too small (distance from the Bering strait to the ice edge is below 100 km) to affect ice breaking and MIZ width, and the variations of fetch are also too small to be related to ice extent. Therefore, most likely, it is the external factor (for example, winter severity) that affects both the ice and sea state.

In July mean and max Hs is proportional to both MIZ area ( $r = 0.6$  and  $0.52$ ) and to the ice area ( $r = 0.43$ ) with a larger number of observations ( $N=13$ ). Being thinner and weaker, ice is more easily breakable by waves in July, therefore we observe wider MIZ (MIZ area above

0.2M km<sup>2</sup>) in years with taller waves (with mean Hs above 1 m and reaching 2 m) whereas in years with lower waves (mean Hs below 0.8) MIZ area is below 0.1M km<sup>2</sup>. The variations of ice extent are still too small in July to affect the fetch and wave height, therefore the observer relation is too weak ( $r=0.43$ ) for a reasonable interpretation.

In the August-September period (green dots on Fig. 2.4.11) the strongest relation between mean and max Hs and sea ice parameters is observed with correlation coefficient reaching 0.8 (N=21). In the years with the smallest ice extent (ice area below 0.6M km<sup>2</sup>) the fetch is the longest (reaching 1000 km from the Bering Strait) and, consequently, the significant wave height is the largest, averaging to 1.4 m and reaching 2.4 m. With the largest ice extent (ice area about 1 M km<sup>2</sup>, fetch below 500 km) the wave height can reach only 1.2 m and averages to 0.8 m. In this period ice area and MIZ area are also highly correlated with  $r=0.86$  (not shown on Figure 2.4.11) suggesting that MIZ is simply a proportion of the total ice and the impact of waves is not seen.

We can summarize that in the Chukchi Sea early in the melting season (June) the preconditioning (e.g. winter severity) plays a more important role in ice and MIZ extent. Later (in July) waves affect ice breakup and wave height can be related to MIZ width. When the ice extent is minimal (August-September) the interannual fetch variations are so large that a clear impact of ice extent on wave height is visible. After the summer season other factors (e.g. strong wind, temperature, currents) play a more significant role in ice breakup and wave buildup and no relation can be observed.

The coincidence of the Hs trends and the correlations between ice extent, MIZ and the sea state in the Chukchi Sea is not random. Clearly, long lasting systematic changes of ice and wave regime are observed in this region and can be extrapolated to other regions and into the future.

### 2.4.3 User Engagement

Regarding user engagement and assessment emphasis will be on the products connected to: (a) trends in the ocean wave climate in the MIZ associated with declining sea ice extent and thickness; and (b) anomalies in the wave field in the MIZ associated with extreme events. These 2 aspects are expected to attract a broader user community which has recently emerged within the Copernicus Services related to climate and the marine environment. Advances in statistical information of the wave climate in the MIZ over the last 25 years is, in particular, expected to be highly relevant for the maritime operators and offshore oil and gas industries. It will also form valuable information for model validations. As such, representatives from these user communities were invited to the first User Consultation Meeting.

## 3. Feedback from Sea State Users

### 3.1 Feedback from the First User Consultation Meeting

#### 3.1.1 Introduction

The first User Consultation Meeting was held on 8-9th October 2019 at the Institut Universitaire Européen de la Mer (IUEM), in Brest, France. It provided a unique opportunity for users of sea state data (scientists, engineers or consultants) to present their work and express their needs regarding a future sea state database in order to increase the benefit to their activities.

This meeting was open to anyone with an interest in sea state, including those working in research and industry on observations, modelling and applications. The meeting featured keynotes, presentations and discussions on the importance and role of Sea State in Earth System Science, on the applications of Sea State and on the scientific requirements for the Sea State Essential Climate Variable.

Full information is available on the UCM website <https://seastatecci-ucm.sciencesconf.org/>

After lunch on the second day, the participants were split into four groups covering relevant themes:

- Climate studies
- Coastal dynamics
- Hindcasting and forecasting
- Marine engineering

Each group spent 45 minutes in discussion on specific aspects including:

- Use of and requirements for Sea State Data
- Importance of uncertainty in the products
- Use of the Sea State CCI dataset
- Comments on UCM meeting

There was then a summary of each discussion in plenary, and the key points for each group are given here.

#### 3.1.2 Group discussion: Climate studies

##### Status

Datasets used by participants consist of remote, in situ and models. It was insisted on the interest of buoys for calibration as well as validation.

- Altimeter data: spatial resolution (intertrack) and temporal resolution (driven by satellite revisit time). It was pointed out the benefit of having a constellation of numerous altimeter missions.

---

Drift can be of the order of cm/yr and is not necessarily corrected in the L2 products, hence the need for reprocessings.

- Buoys data: large heterogeneity between the datasets.

## Requirements

- General: resolution and stability

In term of spatial and temporal resolution no specific values were provided but it was reminded that the best possible resolution is wished

Importance of stability over time was pointed out. We are trying to resolve trends of the order of the cm/year, therefore the drift on wave height measurement should be lower. Homogeneity of the dataset through time over several years is also required. Continuity of the datasets is also important, possible gaps or jumps should be documented.

- Uncertainties

Being provided with a quality flag is one thing, the uncertainty value associated with each data point would be of extra interest.

An example of use was given: being able to derive drift from the uncertainties associated to e.g. 1Hz values of satellite products

- Numerical models:

Documentation about physics packages used, input data (e.g. wind fields...)

Information on how data forcing was ingested in the simulation. Boundary conditions (e.g. bathymetry....)

- Auxiliary data:

It would be interesting to have model data in EO products (e.g. in sat along track products). It was nevertheless stressed that to be useful the model run conditions should be documented in the metadata.

- Documentation and metadata

The importance of having documented products (external documentation as well as in file metadata) was stressed. Consistency of file format between the different datasets is also a plus. NetCDF format with CF compliant attributes and metadata is recommended.

Associated documentation should also mention discontinuities and data that have been lost.

- Data accessibility

Difficulty to find reports about intercalibration techniques and results was pointed out. This is of great interest for multi satellite data use.

This information is also requested for buoys to facilitate inter-comparison between different datasets. Example: instrument averaging period. Need for metadata.

The question of file size / file use was also addressed. A preferred file time length was not specified as it was stated that provided data are in an appropriate format (e.g. NetCDF) they can be concatenated. Data volume can be an issue for download, it would be an advantage to have the possibility to work directly on the platforms hosting the data files.

### 3.1.3 Group discussion: Coastal dynamics

This group was hosted by Graham Quartly and included 5 data providers and 3 data users.

Key points from the discussion were:

1. High resolution data (~100m-1km) is necessary for coastal studies given the rapid evolution of sea states towards the coast;
2. Revisit time period of ~ several days makes it difficult to use altimeter data for coastal studies. Tidal currents strongly affect sea states at the coast and hourly data is often required for coastal process studies;
3. There is a strong interest in spectral information (direction and period) and not only wave height. The use of SAR measurements for coastal studies is still limited;
4. Data users are not well informed about sea state data uncertainties. This information is relevant for assessing model capabilities in coastal regions;
5. Extreme sea level at the coast depends on sea state. Stability of sea state data (wave height and period) is necessary to characterize long term changes in extreme sea levels;

### 3.1.4 Group discussion: Hindcasting and forecasting

This group was hosted by Florian Schlembach and included Paolo Cipollini, 2 modellers and 2 users.

Key points from the discussion were:

1. Issue of models vs. altimeter as the reference. What is the truth, against which source was the altimetry data calibrated? The information is useful because users often use altimeter data for validation
2. Additional uncertainty information would be very useful to provide information for reliability for the measurements
3. Modellers would benefit from wave spectra information in the CCI dataset
  - useful as a reference for validation of new wave models
4. Classifying coastal measurements is of high interest for the users
5. Providing additional uncertainty information is quite expensive. A possible trade-off that could be made: Add multiple levels to quality flag

6. Better characterisation of extreme values for long-time series (for both hindcast and forecast)
7. Link between wave field and other climate indices shall be provided
  - E.g. wave spectra near the coast etc.

### 3.1.5 Group discussion: Marine Engineering

This group was hosted by Ellis Ash and included 6 users and 1 data provider. There was a mix of interests, including:

- offshore conditions for ship design, offshore and renewable energy structures
- coastal conditions for coastal engineering; coastal power stations; erosion control

Key points from the discussion were:

1. Extremes are highly relevant. A long time series (>30 years) is needed for analysis of extremes.
2. Directional wave information is required.
3. Uncertainty is considered relevant, especially for the analysis of extremes, but other factors generally more important are:
  - Sampling
  - Resolution
  - Length of time series

Some users add their own uncertainty values.

4. For coastal engineering projects a resolution of 100m is desired.
5. For erosion and storm surge applications a minimum resolution of 10km is considered suitable.
6. A hindcast model with satellite data assimilation is generally considered the best resource for design.
7. Forecasting is required for storm surge and ship routing applications.

### 3.1.6 Conclusions and recommendations

This first User Consultation Meeting gathered more than 50 researchers and consultants in Brest, France. In order to explore sea state data applications, six topics were defined based on the abstract selection : Instrumentation and Techniques, Spectral Wave Information, Variability and Trends, Coastal Impacts, Extreme Sea States and Numerical Hindcasting and Forecasting. 25 oral presentations were given during the 1.5-day duration of the meeting, and an open discussion session was also scheduled to invite participants to share their

needs and requirements regarding the sea state data they use. Among the most recurrent feedbacks were:

- the need for long-term data to better characterize extreme sea states and trends;
- the importance of spectral information to derive wave direction and wavelength, required for many applications (e.g coastal and marine engineering);
- the limited information on the uncertainty associated with sea state data measured from radar instruments;
- the benefits of adding auxiliary parameters such as along-track model output;
- the necessity to improve data accessibility and documentation;

As regards the requirements on sea state data, we can say that several applications require very high resolution in space (<1km) and time (hourly) that is currently not achievable from EO only. Given that decadal changes in significant wave height are of the order of 1 cm/year, a stability of 1cm / decade seems a reasonable requirement.

For the next meeting, a particular attention should be given to attract more data users, particularly in the climate and modelling community.

### 3.2 Feedback from the Climate Research Group

Five members of the Climate Research Group (Melisa Menendez, Christine Gommenginger, Jean Bidlot, Ian Young and Guillaume Dodet) met at the 2nd International Workshop on Waves, Storm Surges and Coastal Hazards, held in Melbourne, Australia, 10-16 November, 2019, in order to discuss the recent advances of the Sea State CCI project (user feedback on dataset V1.1, round-robin assessment...). Regarding the user feedback on dataset V1.1, it appeared clearly from the interactions at the conference that: 1) there is a strong interest for a sea state Climate Data Record, as implemented within the Sea State CCI project; 2) the wave data users are concerned by consistency issues in long-term wave dataset, such as numerical wave hindcast, wave buoy record and altimeter data; 3) many users are particularly interested in spectral wave information, and look forward to exploring future version of the Sea State CCI dataset.

For the Round-Robin assessment, the CRG provided a number of suggestions to the Algorithm Development team, in charge of computing the metrics for RR exercise, in order to take into consideration several issues raised by the team during previous discussion. These issues were mostly related to the fact that some of the algorithms used some filtering procedure based on neighbouring waveforms and thus could not be directly compared to other algorithms. Also, some algorithms resulted in a strong distortion of the wavenumber spectral variability at scales between 50-500km that required further investigation to provide robust estimates of the global spectral level at these scales.

### 3.3 Links with international wave climate activities

The Coordinated Ocean Wave Climate Project (COWCLIP) is an international collaborative research project, being a component of the work-plan for the JCOMM Expert Team on Waves and Coastal Hazards. Currently coordinated by Mark Hemer (CSIRO), COWCLIP aims to generate wave climate projections at global and regional scales, and aid comprehensive assessments of their cascading uncertainty by providing a systematic, community-based framework and infrastructure to support validation, intercomparison,

documentation and data access for wave climate projections forced from CMIP5 datasets. COWCLIP also aims to engage interests of the wave community into the wider climate community and ultimately develop coupled wind-wave Atmosphere-Ocean global climate models to support quantification of wind-wave driven feedback in the coupled climate system. Finally COWCLIP has implemented a specific task on understanding the historical variability and change of the global wind-wave climate by assessing available global historical datasets (hindcasts, reanalyses, and observational) to determine whether robust signals of historical change or variability can be derived from these datasets. While the first historical dataset to be analysed was Voluntary Observing Ship dataset, COWCLIP has expressed a strong interest in including satellite-based wave information in their analysis. For all these reasons, a strong collaboration between Sea State CCI and COWCLIP is necessary.

A COWCLIP meeting was held on 16 November, after the [2nd International Workshop on Waves, Storm Surges and Coastal Hazards](#), being held in Melbourne, Australia, 10-16 November, 2019. Christine Gommenginger, Jean Bidlot, and Guillaume Dodet, from the Sea State CCI, took part in this meeting. One common objective between Sea State CCI and COWCLIP concerned the determination of a reference wave buoy data set, consistent over time (e.g. with the correction of documented step changes associated to changes in buoy instruments and payloads, see Gemmrich et al, 2010, for instance). Indeed, this effort is particularly relevant for improving the calibration procedure of satellite altimeters.

Another way of strengthening the link between Sea State CCI and COWCLIP was through the integration of the COWCLIP meeting within the next Sea State CCI User Consultation Meeting. Several COWCLIP participants manifested their interest in the UCM although the date and location was a potential obstacle for this initiative. One suggestion was to organize a combined COWCLIP/CCI UCM meetings in the continuity of the OSTST, to be held in Venice on 19-23 October 2020. These issues will be discussed at the next Sea State CCI Progress Meeting.

## 3.4 Feedback from the Second User Consultation Meeting

### 3.4.1 Introduction

The second User Consultation Meeting was held on 23rd-25th March 2021 as a fully online meeting via WebEx. There were ten keynote presentations to show off the CCI dataset and the many varied disciplines providing or relying on sea state data (whether from satellites or buoys or other in situ information). These were accompanied by a further nineteen talks and five posters to showcase the breadth of work. (Posters were displayed via the Padlets app, allowing message-board style interaction between the various readers and the authors.



### 3.4.2 Diversity of Audience

The meeting was spread over 2.5 days (9am to 5pm UK time), which meant that not all the sessions were at convenient times for people in far-off countries; however it did enable a greater attendance on a part-time basis. There were over 170 people registered for the meeting, with individual sessions getting between 40 and 70 online attendees. Since there was no need for travel, the meeting attracted speakers from U.S., Canada, Australia and Russia as well as many parts of Europe, and we were able to hold keynote sessions with various speakers from industry who might not have been able to spare the time for an in-person meeting.

### 3.4.3 Interaction

Sessions were organised with 40 minutes for keynote presentations; 25 minutes for other speakers. These were slightly longer slots than used for some other online meetings, but meant that nearly all talks did allow time for at least 5 minutes questioning, rather than having rushed handovers between speakers. As there were no opportunities for informal discussions on a one-to-one basis, we strongly encouraged people to partake in an online questionnaire to gauge their level of interest and experience with various satellite products. The results of this questionnaire were shared in the last session of the meeting

### 3.4.4 Feedback

There was significant discussion with participants as to which products they considered important and the desired coverage and spatial resolution. This was complemented by an online survey that ran from the start of the meeting to several months later in order to get the widest degree of response. The full analysis is detailed in v3 of the URD, but a few key points are listed here. There were 92 participants from 25 different countries, and although 30% felt satellite data were essential for their work, there was 14% who had never used satellite data. This indicates that we were reaching out to some degree to a different audience from the prior in-person UCM.

The parameter most sought after by this community was significant wave height, followed by wind and full 2D wave spectrum. As many of the respondents were interested in hourly data or fine resolution, there was a significant proportion who found the sampling of the current datasets to be a limiting factor in their use. (Note, a higher proportion of these people used ECMWF reanalysis than had used Sea state CCI products.) There was strong community interest in wave data in the coastal zone, and, to a lesser extent, in the polar oceans.

## 4. References

- Abdalla , S., P. A. E. M. Janssen & J.-R. Bidlot (2011) Altimeter Near Real Time Wind and Wave Products: Random Error Estimation, *Marine Geodesy*, 34:3-4, 393-406, <https://doi.org/10.1080/01490419.2011.585113>
- Cipollini P and A Shaw (2017) ESA: Sea Level Climate Change Initiative Project. WP2710-WP2740: Assessment of Specialized Retracking in the Coastal Zone. ESRIN Contract No. 4000109872/13/I-NB
- Dodet, G., Bertin, X., Taborda, R., 2010. Wave climate variability in the North-East Atlantic Ocean over the last six decades. *Ocean Modelling* 31, 120–131. <https://doi.org/10.1016/j.ocemod.2009.10.010>
- Hemer, M.A., Church, J.A., Hunter, J.R., 2010. Variability and trends in the directional wave climate of the Southern Hemisphere. *International Journal of Climatology* 30, 475–491. <https://doi.org/10.1002/joc.1900>
- Hochet, A., Dodet, G., Ardhuin, F., Hemer, M., Young, I., 2021. Sea State Decadal Variability in the North Atlantic: A Review. *Climate* 9, 173. <https://doi.org/10.3390/cli9120173>
- Hu, S., Sprintall, J., Guan, C., McPhaden, M.J., Wang, F., Hu, D., Cai, W., 2020. Deep-reaching acceleration of global mean ocean circulation over the past two decades. *Science Advances* 6, eaax7727. <https://doi.org/10.1126/sciadv.aax7727>
- Hussain et al., (2019). pyMannKendall: a python package for non parametric Mann Kendall family of trend tests, *Journal of Open Source Software*, 4(39), 1556, <https://doi.org/10.21105/joss.01556>
- Piolle JF , Dodet. G and E. Ash: Sea State CCI Product User Guide v 1.0 , 17 January 2020.
- Reguero, B.G., Losada, I.J., Méndez, F.J., 2019. A recent increase in global wave power as a consequence of oceanic warming. *Nature Communications* 10. <https://doi.org/10.1038/s41467-018-08066-0>
- Ribal, A., Young, I.R., 2019. 33 years of globally calibrated wave height and wind speed data based on altimeter observations. *Scientific Data* 6, 77. <https://doi.org/10.1038/s41597-019-0083-9>
- Shimura, T., Mori, N., Mase, H., 2013. Ocean Waves and Teleconnection Patterns in the Northern Hemisphere. *Journal of Climate* 26, 8654–8670. <https://doi.org/10.1175/JCLI-D-12-00397.1>
- Stopa, J.E., Cheung, K.F., 2014. Periodicity and patterns of ocean wind and wave climate. *Journal of Geophysical Research: Oceans* 119, 5563–5584. <https://doi.org/10.1002/2013JC009729>
- Stopa, J.E., Ardhuin, F., Girard-Ardhuin, F., Wave climate in the Arctic 1992-2014: seasonality and trends, *The Cryosphere*, 10, 1605-1629, 2016
- Timmermans, B.W., Gommenginger, C.P., Dodet, G., Bidlot, J.-R., 2020. Global Wave Height Trends and Variability from New Multimission Satellite Altimeter Products, Reanalyses, and Wave Buoys. *Geophysical Research Letters* 47, e2019GL086880. <https://doi.org/10.1029/2019GL086880>
- Timmermans, B.W., Shaw AGP, Gommenginger C. Reliability of extreme significant wave height estimation from satellite altimetry and in situ measurements in the coastal zone. *Journal of Marine Science and Engineering*. 2020 Dec;8(12):1039. <https://doi.org/10.3390/jmse8121039>

Schlembach F, Passaro M, Quartly GD, Kurekin A, Nencioli F, Dodet G, Piollé JF, Arduin F, Bidlot J, Schwatke C, Seitz F. Round robin assessment of radar altimeter Low Resolution Mode and delay-Doppler retracking algorithms for significant wave height. *Remote Sensing*. 2020 Jan;12(8):1254. <https://doi.org/10.3390/rs12081254>

URD Sea State CCI User Requirements Document v2 (Jun 2021)

Vanem, E. (2017). *A regional extreme value analysis of ocean waves in a changing climate*. *Ocean Engineering*, 144, 277–295. <https://doi.org/doi:10.1016/j.oceaneng.2017.08> .

Young, I.R., Ribal, A., 2019. Multiplatform evaluation of global trends in wind speed and wave height. *Science* 364, 548. <https://doi.org/10.1126/science.aav9527>

Zhang, X., Church, J.A., 2012. Sea level trends, interannual and decadal variability in the Pacific Ocean. *Geophysical Research Letters* 39. <https://doi.org/10.1029/2012GL053240>